



Sandia National Laboratories

Operated for the United States Department of Energy
by National Technology and Engineering Solutions
of Sandia, LLC.
Albuquerque, New Mexico 87185-0747
Livermore, California 94551

date: 15 November 2019

to: Paul Shoemaker, 8880
Todd Zeitler, 8863
Ross Kirkes, 8883

from: Rob P. Rechard, 8842
Emily Stein, 8843

subject: Hydrologic and Geochemical Constraints on Criticality in Geologic Media Near Bedded Salt Repository

ABSTRACT

This paper presents the rationale for why hydrologic and geochemical constraints prevent a critical event from occurring sometime in the future after closure of the Waste Isolation Pilot Plant (WIPP), an operating repository in southeastern New Mexico for the geologic disposal of wastes containing transuranic radioisotopes from atomic energy defense activities. In the past, concern about criticality in transuranic waste has been low because of the low initial concentration of fissile material and the natural tendency of fissile solute to disperse during transport. The potential disposal of other waste types with high initial concentrations of fissile material necessitates a renewed evaluation of the criticality potential, even though the container fissile mass remains low. The fairly uniform distribution of iron in the containers and magnesium oxide added in the disposal drifts, keeps the brine chemistry uniform such that pH, ionic strength, and reduction-oxidation potential do not vary widely, on a macroscopic scale, and cause fissile deposition in preferential regions of the repository. Hydrologic constraints limit fissile deposition to the Culebra dolomite strata above the repository after a hypothetical inadvertent intrusion into WIPP. The typically low solubility of the fissile material implies that vast amounts of brine are required to transport a sufficient quantity of fissile material to the Culebra dolomite to cause criticality. The large amount and variability of the brine flux spreads out the mixing zone where precipitation and colloid aggregation might occur through changes in ionic strength and pH. The subsequently large mixing zone is such that a concentration of fissile plutonium greater than a criticality limit of 3.7 kg/m³ cannot be reached. In addition, the adsorptive capacity of dolomite is mostly through ion exchange of metal cations, such as calcium and magnesium, that must be dislodged by fissile plutonium. The competition of fissile plutonium with calcium and magnesium ions in Culebra brine is such that adsorption would not contribute much to deposition. Finally, thermodynamic equilibrium of the dissolved fissile concentration with any colloids within a small destabilization/filtration region limits the ability of colloids to exceed the solution concentration by orders of magnitude.

I. INTRODUCTION

As with other nuclear facilities, the possibility of sufficient fissile mass and concentration causing a self-sustained neutron chain reaction (criticality) must be evaluated for geologic disposal systems both during operations and after closure. This report relates to the potential of criticality sometime in the future after closure of the Waste Isolation Pilot Plant (WIPP), an operating repository in bedded salt in southeastern New Mexico for the geologic disposal of wastes containing transuranic (TRU) radioisotopes from atomic energy defense activities.

In the past, concern about criticality in TRU waste has been low because of the low initial concentration of fissile material and the natural tendency of fissile solute to disperse during transport, as discussed in 2001 and summarized in 2015.¹⁻³ However, waste destined for WIPP has expanded to include other TRU waste with high initial concentration (although low fissile mass).⁴ Hence, a renewed evaluation of the criticality potential was undertaken.

The update is divided into three parts: evaluation of (1) neutronic criteria necessary for criticality in geologic media, as discussed in a companion memorandum;^{5; 6} (2) hydrologic and geochemical aspects that prevent fissile material from assembling into critical concentrations, which is discussed here, and (3) physical compaction of containers in the disposal rooms through salt creep, as discussed in a second companion memorandum.⁷ In combination, these documents support eliminating criticality events from consideration in performance assessments of WIPP.

I.A. Performance Criteria for Waste Disposal at WIPP

In response to the *Nuclear Waste Policy Act (NWPA) of 1982*,⁸ the US Environmental Protection Agency (EPA) promulgated the radiation protection standard, 40 CFR 191 in 1985.^{9; 10} In 40 CFR 191, EPA requires a performance assessment (PA) to assess whether pertinent features, events, and processes (FEPs) included in a radioactive waste disposal system meet regulatory performance limits.^a The primary health indicator is the cumulative release of radionuclides. In the *WIPP Land Withdrawal Act of 1992*,¹¹ Congress directed that EPA implement the long-term disposal standards at WIPP. In response, EPA promulgated WIPP-specific certification criteria in the implementing regulation, 40 CFR 194, in 1996.^{12; 13} In 40 CFR 194, EPA requires that DOE document the continued compliance of WIPP with 40 CFR 191 every 5 years, which might include an updated PA that incorporates pertinent new information. The information and results presented here consider inventory, repository design, and PA modeling changes related to criticality for the 2019 Compliance Recertification Application (CRA-2019).

I.B. Criticality Scenario Class

In a geologic repository, the criticality phenomenon can be categorized either as an event or as a long-term process. One speaks of a critical event and a corresponding event class when the emphasis is on an initiating event, such as inside a waste container after an accident during operations. Here, however, we speak of a criticality scenario class because the emphasis is on features and processes in the near- and far-field of the disposal system acting to assemble a critical configuration of fissile mass after closure of the repository.

^a In this context, a feature is an aspect or condition of the disposal system, an event is a short-term natural or anthropogenic phenomenon, and a process is a long-term natural phenomenon (i.e., a phenomenon that occurs over a major portion of the regulatory period).

EPA does not provide separate guidance regarding the occurrence of post-closure criticality in either 40 CFR 191 nor 40 CFR 194. Rather, criticality is considered along with other FEPs and scenario classes of the disposal system.^b A probabilistic framework for evaluating criticality after closure of the repository, where humans are separated from a hypothetical event by up to 600 m of salt differs substantially to screening criticality during operations when humans are present. During operations, the rationale for eliminating the need to consider criticality is rule-based (ANSI/ANS-8.1) whereby several worse-case scenarios of assembling fissile material are developed and then calculations made to demonstrate the impossibility of criticality in order to ensure safety to nearby humans.¹⁶

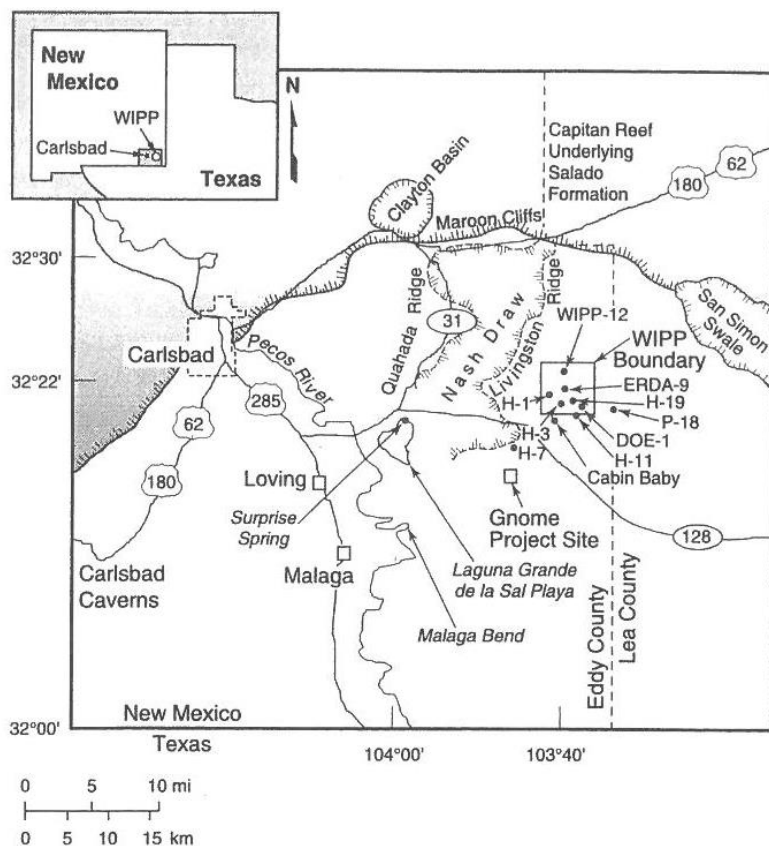


Fig. 1. The WIPP repository, located in the Delaware Basin of the Permian Basin in southeastern New Mexico, is ~40 km east of Carlsbad..^{1, Fig. 1}

I.C Approach for Screening Criticality at WIPP

A rationale for omitting the criticality event was developed as part of the Compliance Certification Application (CCA) submitted to the US Environmental Protection Agency (EPA) in October 1996 (CCA-1996)^{13; 17; 18} and approved in May 1998.¹⁹ Although the CCA-1996 included a low-consequence rationale to show the overall risk was very low (as summarized in 2015),^{2; 3} the CCA-1996 primarily developed a *qualitative* low-probability rationale to exclude criticality in the underground facility and in formations above the underground facility based on arguments

^b In the site-specific Standard for the Yucca Mountain repository (40 CFR 197),^{14; 15} EPA did not identify criticality for special consideration when evaluating the post-closure behavior even though EPA had the opportunity to do so when EPA used criticality as a FEP screening example in the preamble for 40 CFR 197.

that no physical, hydrologic, or geochemical mechanisms exist for sufficiently concentrating fissile ^{239}Pu and ^{235}U radionuclides.² This approach is followed here also.

I.D. Implications of Repository Design and Modeling Changes since CCA-1996

The criticality screening discussed here uses the 2019 Compliance Recertification Application (CRA-2019) PA. CRA-2019 builds upon the 2017 analysis of the abandonment of panel closures in the south of the disposal region (APCS-2017). Specifically, APCS-2017 analyzed DOE’s plan to abandon waste emplacement in equivalent Panel 9 and panel closures between filled Panels 3, 4, 5, and 6 in the south end of the underground facility—see §III).²⁰ In turn, the APCS-2017 builds upon CRA-2014. The lack of panel closures in the south end causes increased pressures and saturations, which lead to increase releases to the Culebra Dolomite Member of the Rustler Formation. Furthermore, brine moving through the repository has access to more of the repository. Hence, more mixing of waste components can occur after human intrusion. Even prior to a human intrusion, some mixing of surplus Pu disposed in new panels in the north with existing waste in the southern panels may occur because of the slight 1° dip of the strata.

More importantly, an increase in the modeled solubility of Pu^{III} and Pu^{IV} in Castile brines and a significant increase in the corresponding uncertainty of Pu^{III} solubility have occurred since CCA-1996. Consequently, the amount of brine and Pu moving through the repository and up an abandoned intrusion borehole noticeably increased in a few outlying simulations of CRA-2019 compared to CCA-1996.

These design and modeling changes alter the rationale for omitting criticality after extensive degradation of containers. These changes have had a much greater influence on the rationale than changes in the amount of Pu disposed at WIPP. Release of Pu at WIPP is solubility controlled; hence, changes in the Pu inventory does not directly influence Pu release.

II. OVERVIEW ON SCREENING CRITICALITY

Evaluating the potential for criticality after closure of WIPP is done within the probabilistic regulatory framework for disposal.^{9; 10}

II.A. Expected Cumulative Release Measure

In the long-term disposal standards in 40 CFR 191, the primary health indicator is the cumulative release of radionuclides $R_{total}(\mathbf{p})$ and where \mathbf{p} is the set of model parameters and its measure is the expected cumulative release at a compliance boundary normalized by the repository size and EPA specified release limits. More specifically,^{9; 10}

$$\bar{R}_{total} = E\{R_{total}(\mathbf{p})\} \quad (1)$$

where^{21, App. B}

$$R_{total}(\mathbf{p}) = \sum_{r=1}^{n_r} \frac{1}{f_w L_r} Q_r(\mathbf{p}) \quad (2)$$

$$= \sum_{r=1}^{n_r} \frac{1}{f_w L_r} \int_0^{\infty} \oint_{x^{ae}} \mathcal{M}_r(t, \mathbf{x}; \mathbf{p}) dx dt \quad (3)$$

where f_w is a waste unit factor equal to $\sum W_r/10^6$ Ci for WIPP; W_r is total activity (Ci) in the repository of α -emitting transuranic (TRU) radionuclides r with half-life ($t_r^{1/2}$) ≥ 20 years; L_r is the regulatory release limit (Ci) for radionuclide

r specified in 40 CFR 191; and Q_r is cumulative release over the regulatory period \mathfrak{T} (10^4 yr) for radionuclide r at the boundary of the disposal system x^{ae} .

II.B. Human Intrusion.

In 40 CFR 191 and 40 CFR 194,^{9; 10; 22} EPA requires the DOE to demonstrate that the WIPP will comply with the performance criteria after hypothetical human intrusion into the repository. However, EPA narrowed the focus of interest for speculative anthropogenic disruption to that of inadvertent exploratory boreholes into the repository using present drilling technology.¹⁵ As demonstrated the first PA in 1989 and thereafter,^{13; 23-25} without human intrusion to disrupt and allow brine to pass through the repository, there is no large driving force for the movement of radioisotopes; hence, the human intrusion scenario is fundamental to the movement and assembly of fissile material beyond the repository.

The short-term result of intrusion is entrainment of wastes into the drilling fluid and their immediate release at the surface. At later times, releases may occur through the abandoned borehole. In the stylized calculation, the borehole, filled with material that has the permeability of silty sand, creates an advective path from the repository to an aquifer (in comparison to diffusion through the salt) but retains the remainder of the natural barrier in the aquifer, where transport of radionuclides might be dispersed.

II.C. Scenario Classes of WIPP PA

The \bar{R}_{total} in Eq. (1) can be expanded to include the expectation from aleatoric \mathbf{a} and epistemic \mathbf{e} uncertain parameters (i.e., $\mathbf{p} = \{\mathbf{e}, \mathbf{a}\}$)^c

$$\bar{R}_{total} = \mathcal{E}\{R_{total}(\mathbf{p})\} = \mathcal{E}^E\{\mathcal{E}^A\{R_{total}(\mathbf{e}, \mathbf{a})\}\} \quad (4)$$

For the WIPP repository, 6 major scenario classes can be formed from the aleatoric uncertainty:^{23, Fig. 3.2-2; 26, Table 6} undisturbed conditions (\mathcal{A}_U); drilling intrusion through repository to underlying brine pocket in the Castile Formation (described in §III) (\mathcal{A}_{E1}); intrusion into only the repository (\mathcal{A}_{E2}), and two intrusions one of which intersects an underlying pressurized brine pocket (\mathcal{A}_{E2E1}); subsidence in the formation above the repository caused by potash mining (\mathcal{A}_{TS}); and criticality (\mathcal{A}_C).

The expected cumulative release consequence is the sum of the 6 incremental consequences when approximating the aleatoric expectation with the 6 scenario classes:

$$\bar{R}_{total} = \mathcal{E}^E\left\{\sum_{j=1}^{n_A=6} R_{total}(\mathbf{e}, \mathbf{a}_j)\mathcal{P}\{\mathbf{e}, \mathbf{a}_j\}\right\} \quad (5)$$

$$= \sum_{j=1}^{n_A=6} \bar{R}_j \quad (6)$$

$$= \bar{R}_U + \bar{R}_{E1} + \bar{R}_{E2} + \bar{R}_{E2E1} + \bar{R}_{TS} + \bar{R}_C \quad (7)$$

^c Epistemic parameters are associated with the probability models and exposure models but the distinction is not necessary here (i.e., $\mathbf{p} = \{\mathbf{e}^p, \mathbf{e}^e, \mathbf{a}\}$)

$$\approx \bar{R}_U + \bar{R}_{E1} + \bar{R}_{E2} + \bar{R}_{E2E1} + \bar{R}_{TS} \quad (8)$$

Eq. (8) is a valid approximation for \bar{R}_{total} if the incremental consequences from criticality scenario class (\bar{R}_C) are so small relative to consequences from the other scenario classes that it is not necessary to consider based on EPA guidance.

II.D. Criteria for Screening Criticality Scenario Class

In Appendix C of 40 CFR 191^{9, 10} and in 40 CFR 194.32,^{12, 13} the EPA gives three criteria for excluding FEPs or a scenario class such as criticality from the performance assessment over the 10,000-year regulatory period: (1) regulatory fiat; (2) low probability of occurring; and (3) low consequence. Regulatory fiat includes guidance excluding purposeful mining of the repository. Exclusion of low probability FEPs and scenario classes is via (a) qualitative rationale that the FEPs and scenario classes are not credible based on site, waste, or repository characteristics or (b) a quantitative demonstration that the probability is $<10^{-4}$ over 10^4 years.^{9, Appendix B; 10, Appendix C} Exclusion of low consequence FEPs and scenario classes is via (a) a reasoned rationale that inclusion of a FEP/scenario class would not influence timing or magnitude of the performance measure in a non-conservative manner, or (b) a calculation demonstrating that the change in performance measure (or a secondary intermediate measure) is sufficiently small when including the FEP/scenario class.

To use the EPA probability or consequence screening criteria requires expanding \bar{R}_C into its probability and consequence components, using several approximations implied in EPA regulatory guidance. By analogy with Eq. (4),

$$\bar{R}_C = \mathcal{E}^E \{ \mathcal{E}^A \{ R_C(\mathbf{e}, \mathbf{a}) \} \} \quad (9)$$

Approximating the aleatoric expectation of criticality by summing computational scenarios yields

$$= \mathcal{E}^E \left\{ \sum_{k=1}^{n_{CS}} R_C(\mathbf{e}, \mathbf{a}_k) \phi\{\mathbf{e}, \mathbf{a}_k\} \right\} \quad (10)$$

$$= \mathcal{E}^E \left\{ \sum_{k=1}^{n_{CS}} R_k^{CS}(\mathbf{e}) \phi\{\mathcal{A}_k^{CS}\} \right\} \quad (11)$$

where Eq. (11) presents an alternative notation for Eq. (10). No sharp distinction exists between the coarse criticality scenario class and computational scenarios; rather a continuum exists. Here, the terms distinguish between broad category of futures useful for organizing the analysis and fine groupings of futures useful for computations.

EPA guidance implies that epistemic means of the probability and consequences of FEPs and scenario class provide an adequate estimate for screening,^d hence,

^d The use of the mean probability for screening FEPs is emphasized by NRC in the Yucca Mountain Review Plan (YMRP)^{27, 22-14} "...the mean of the distribution range is to be used to screen an event from the performance assessment." Consequently, the WIPP Project does not present a distribution for the probability of criticality.

$$\approx \sum_{k=1}^{n_{CS}} \bar{R}_k^{E, CS}(\mathbf{e}) \bar{\phi}^E \{ \mathcal{A}_k^{CS} \} \quad (12)$$

$$< \left(\sum_{k=1}^{n_{CS}} \bar{R}_k^{E, CS}(\mathbf{e}) \right) \cdot \sum_{k=1}^{n_{CS}} \bar{\phi}^E \{ \mathcal{A}_k^{CS} \} \quad (13)$$

$$= \bar{R}_C^{E, CS}(\mathbf{e}) \cdot \bar{\phi}^E \{ \mathcal{A}_C \} \quad (14)$$

The inequality of Eq. (13) and its alternative notation in Eq. (14) assumes the expectation can be sufficiently approximated for the purposes of screening by the product of the sum of the consequences and the sum of the scenario class probabilities, without considering any potential interplay between the individual conditional consequence $\bar{R}_k^{E, CS}(\mathbf{e})$ and the probability $\bar{\phi}^E \{ \mathcal{A}_k^{CS} \}$ (e.g., the evolution of the criticality consequences is reasonably independent of the probability of the criticality computational scenarios, which is only approximately true on a macroscale). The sum of the probabilities of the computational scenarios of criticality is of most interest here:

$$\bar{\phi}^E \{ \mathcal{A}_C \} = \sum_{k=1}^{n_{CS}} \bar{\phi}^E \{ \mathcal{A}_k^{CS} \} \quad (15)$$

II.E. Computational Scenarios Considered for Screening Criticality at WIPP

Two environmental conditions (e) were considered for defining the computational scenarios considered for the criticality screening at WIPP in Eq. (15): (1) the undisturbed condition ($e \sim U$) and (2) the condition after inadvertent human intrusion ($e \sim H$) (i.e., for criticality screening, general intrusion is sufficient rather than using the three types adopted for the PA (\mathcal{A}_{E1} , \mathcal{A}_{E2} , and \mathcal{A}_{E2E1})),

The potential for criticality was also evaluated primarily at two feature locations of the disposal system (f): (1) the underground repository ($f \sim R$), and (2) the Culebra in the natural geologic barrier ($f \sim GB$). Other locations briefly considered in the geologic barrier were the disturbed rock zone around the repository, anhydrite marker beds in the Salado, and the small diameter abandoned exploratory borehole. However, these locations will not be numerated here since the amount of contaminated brine inflow (and subsequent fissile deposition) is bounded by fluid flow in the repository and into the Culebra such that the probability of criticality was much less than the two locations numerated here.^{1, §IV.B; 2, §3.5}

Location is not usually a convenient means of defining a scenario class in a PA since location is not associated with aleatoric uncertainty; rather, the likelihood of radionuclides such as fissile material residing in a specific location is modeled as part of epistemic uncertainty. However, here it useful to subdivide the criticality scenario class by location even though it is not possible to assign a distinct probability by location. The probability of fissile material in both the GB and RP (i.e., $\phi \{ E_{GB} \}$ and $\phi \{ E_R \}$) is eventually approximately one, but the probabilities do differ in the first 10^4 yr.

A third criticality computational scenario class considered is the contribution to probability from various phenomena/processes (p) such as physical compaction, precipitation, adsorption, and colloidal filtering.

A fourth criticality computational scenario class considered was based on four container types (c) to account for different packaging. The container types are only important in the underground facility prior to extensive degradation of the WIPP containers because Pu release to the geologic barrier is solubility controlled except at extreme Pu solubility (as discussed in §V).

In summary, we notionally discuss the low probability rationale as sum of probabilities from these 4 components.

$$\begin{aligned} \bar{\phi}^E \{ \mathcal{A}_C \} &= \sum_{k=1}^{n_{CS}} \bar{\phi}^E \{ \mathcal{A}_k^{CS} \} \\ &= \sum_c \bar{\phi}^E \{ \mathcal{A}_{U,R,compact,c}^{CS} \} + \sum_e^{U,H} \sum_f^{R,GB} \sum_p^{precip,adsorp,filter} \bar{\phi}^E \{ \mathcal{A}_{e,f,p}^{CS} \} \end{aligned} \quad (16)$$

A companion memorandum discusses the first summation on container compaction.⁷ This memorandum focuses on the second summation of hydrologic and geochemical constraints on precipitation, adsorption, and colloidal aggregation/filtering preventing criticality. The rationale for subcritical conditions within the repository (RP) before and after intrusion are very similar and so conceivably the second summation could be simplified (i.e.,

$\sum_f^{RP,GB} \sum_p^{precip,adsorp,filter} \bar{\phi}^E \{ \mathcal{A}_{H,f,p}^{CS} \}$); however, the distinction before and after intrusion has been retained in this memorandum.

The use of computational scenarios in Eq. (16) to determine the total probability of criticality is strictly true only for disjoint (mutually exclusive) computational scenarios. While the environment (undisturbed condition and human intrusion event) and container types are disjoint, the locations and processes considered are not. Here, it is a notional construct to organize the various arguments in the rationale.

In addition, the total probability of criticality at WIPP, as defined in Eq. (16), can be expanded and displayed as a pathway to criticality (Fig. 2):

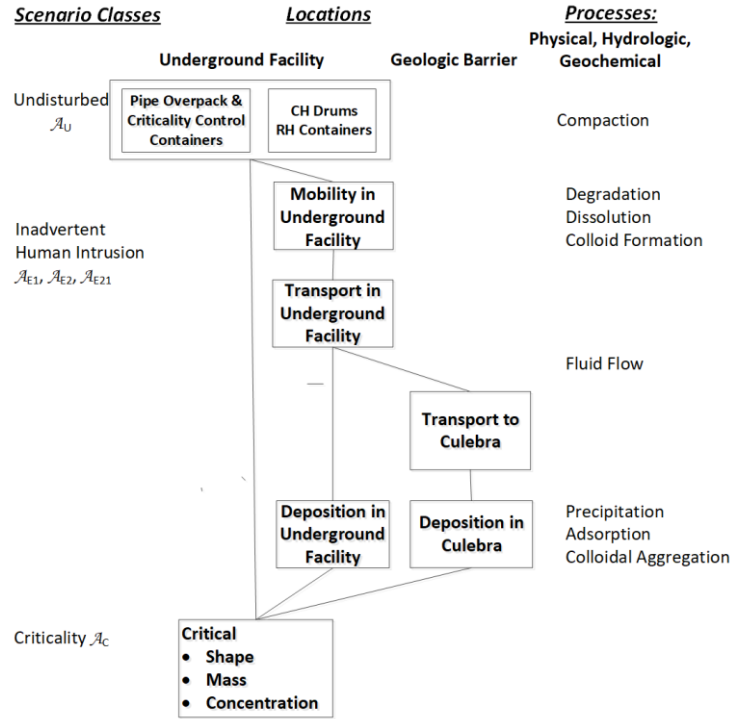


Fig. 2. Pathways to criticality at WIPP

II.F. Approximation of Mean Probability

The mean with respect to the epistemic uncertainty (i.e., $\bar{\phi}^E \{ \mathcal{A}_k^{CS} \}$) is not formally evaluated for screening the criticality scenario class but rather approximated. One approach is to use calculations that represent typical behavior. The intent is to argue that because criticality cannot occur for a representative calculation that the probability of criticality is qualitatively very small.

A related second approach is to use bounding results from the CRA-2019 to argue that the probability was very small. However, the purpose was not to produce a bound on the distribution of the probability of the criticality scenario class (i.e., $\max \phi \{ \mathcal{A}_C \}$) but rather ensure that the lack of criticality did indeed bound the mean probability and would do so in the future even with possible changes in repository design, containers, and Pu solubility.

A third approach is to use mean or representative parameters in functional relationships. Granted using mean parameters in a functional relationship does not imply that the mean of the function is calculated if the function is nonlinear. Fortunately, the criticality class probability is the sum of computational probabilities that are often the product of several factors (as represented by branches in an event tree). In turn, the factors involve very small parameters such that most of the expressions can be linearized as the sum and product of factors. Hence, the mean values can provide a good estimate of the mean of the total probability (i.e., $\bar{\phi}^E \{ \mathcal{A}_k^{CS}(\mathbf{e}) \} \approx \phi \{ \mathcal{A}_k^{CS}(\bar{\mathbf{e}}) \}$) where $\bar{\mathbf{e}}$ represents the expected value of each of the parameters of \mathbf{e}).

III. WIPP Disposal System

As discussed here, the likelihood of assembling a critical mass in or near a repository after closure depends upon (1) the type, form, and initial masses of fissile material (as discussed in this section); (2) the location and type of host

geology, which determine the hydrologic and geochemical process present in the disposal system (as discussed in this section); and (3) the ability of the hydrologic and geochemical processes to concentrate enough fissile mass to meet the criteria necessary for occurrence of the criticality scenario (as discussed in the remainder of the paper).

III.A. Transuranic Waste

III.A.1. General Categories of TRU Waste.

The two primary types of TRU waste destined for WIPP are¹³ (1) contact-handled transuranic (CH-TRU) waste, which is TRU waste with an external dose rate <0.56 $\mu\text{Sv/s}$ (200 mrem/h), and (2) remotely handled transuranic (RH-TRU) waste, which is >0.56 $\mu\text{Sv/s}$ but <2.8 mSv/s (1000 rem/h). The standard waste form of CH-TRU has consisted of a variety of organics, inorganics, and solidified materials contaminated by α -emitting TRU radionuclides generated from atomic energy defense activities.

The projected average ²³⁹Pu enrichment for CRA-2019 is 90%; for CRA-2014, 76%; for CRA-2009, 92%; CRA-2004, 95%, and for CCA-1996, 90%. The projected average ²³⁵U enrichment at emplacement for CRA-2019 is 2.3%; for CRA-2014, 15.5%; for CRA-2009, 2.5%; for CRA-2004, 0.38%; and for CCA-1996, 5.3%.

Table I. Projected fissile material in 2033 for past re-certifications of WIPP

Radioisotope	CCA-1996 ^a (kg)	CRA-2004 ^b (kg)	CRA-2009 ^c (kg)	CRA-2014 ^d (kg)	CRA-2019 ^e (kg)
Uranium (CH&RH)					
²³³ U	202	132	21.4	14.4	13.2
²³⁴ U	81.8	51.3	49.8	39.0	78.4
²³⁵ U	8 070	1 050	2 080	35 400	2 970
²³⁶ U	6.64	25.5	24.7	84.2	10.5
²³⁸ U	149 000	460 000	81 600	193 000	126 000
Enrichment (²³³ U+ ²³⁵ U)	5.3%	0.26%	2.5%	15.5%	2.3%
Plutonium (CH&RH)					
²³⁸ Pu	114	73.2	86.2	35.1	56.3
²³⁹ Pu	12 800	10 700	8 270	9 260	14 100
²⁴⁰ Pu	944	477	639	771	1 410
²⁴¹ Pu	4.01	5.22	4.95	6.44	18.1
²⁴² Pu	298	6.91	19.3	2060	41.7
²³⁹ Pu fissile kg mass equivalent ^f	18 200	11 500	9 660	32 100	16 100
Enrichment ²³⁹ Pu	90%	95%	92%	76%	90%

^aRef¹⁸, Appendix BIR Revision 3

^bRef²⁸; CRA-2004 PABC for EPA has somewhat different masses but change does not effect PA²⁸

^cRef²⁹

^dRef³⁰

^eRef³¹

^fThe Pu fissile mass equivalence (FME) is the mass of ²³⁹Pu plus various factors of the masses of 0.113²³⁸Pu, 0.0225²⁴⁰Pu, 2.25²⁴¹Pu, 0.0075²⁴²Pu, 0.9²³³U, 0.643²³⁵U, ²³⁷Np, 0.0187²⁴¹Am, 34.6^{242m}Am, 0.0129²⁴³Am, 15²⁴⁵Cm, 0.5²⁴⁷Cm, 45²⁴⁵Cf, and 90²⁵¹Cf.

II.A.2. Excess Non-Pit Plutonium

As part of the 1991 Strategic Arms Reduction Treaty (START I) with Russia to dismantle ~80% of strategic nuclear weapons, the US Department of Energy (DOE) identified ~51.7 MT of surplus Pu in various stages of manufacturing at several sites for disposition in the 1996 Programmatic EIS. DOE decided in 2011 to process the ~0.6 MT of miscellaneous Pu and send it to WIPP. In 2012, DOE proposed, and in 2016, DOE selected disposal of the 6.0 MT of non-pit Pu inventory at WIPP and subsequently added it to the WIPP inventory for CRA-2019;⁴ however it has

not yet been shipped. Because bounding estimates were used in CCA-1996, and because estimates for CRA-2004 and thereafter greatly decreased the ^{239}Pu inventory, the disposal of 6.6 MT represents only a small increase in ^{239}Pu and the Pu fissile mass equivalence is still less than originally planned in 1996.

III.A.3. TRU Containers

For disposal in a salt repository, the function of the packaging is to allow for retrievability of the waste during operations, not to retain the waste after closure of the salt repository (i.e., if the waste can be shipped it can be disposed provided social-political agreements in the *WIPP Land Withdrawal Act* are met). None of the containers used at WIPP act as an engineered barrier to release in a brine environment. This memorandum focuses on conditions after substantial degradation of the containers.

About 54% of CH-TRU is disposed in 7-packs of 55-gallon drums but CH-TRU also is disposed in 7-pack pipe overpack containers (15%), standard waste metal boxes (8%), and 10-drum overpacks (4%). Super-compacted CH-TRU waste comes in 3-pack 100-gallon drums (19%). A few shipments have used 3-pack 85-gallon drums. Future shipments of non-pit Pu may come 7-pack criticality control containers. Originally, all RH-TRU was to arrive in canisters and be emplaced in the repository walls (ribs). While some RH-TRU may still arrive in canisters, much RH-TRU waste may come in shielded overpack containers and disposed in the excavated rooms in the future.

III.B. Geologic Characteristics of WIPP Disposal System

III.B.1. Castile Formation

The 500-m-thick Castile Formation, the lowest strata discussed here, consists of three anhydrite (CaSO_4) members and two interspersed halite (NaCl) members (Fig. 3). Within the land-withdrawal boundary of WIPP (Fig. 1), a pressurized brine reservoir was intersected in the fractured Anhydrite III layer of the Castile by one exploratory borehole (WIPP-12) during site characterization (Fig. 3).^{18, Appendix DEL, Section 7.5} The disposal area was moved 1.8 km south, but the presence of a brine pocket beneath the disposal area could not be dismissed; hence, WIPP PAs assume (1) a pressurized brine reservoir exists in the Castile beneath a portion of the repository, and (2) Castile brine could enter the repository through a new exploratory borehole in the next 10 000 years.

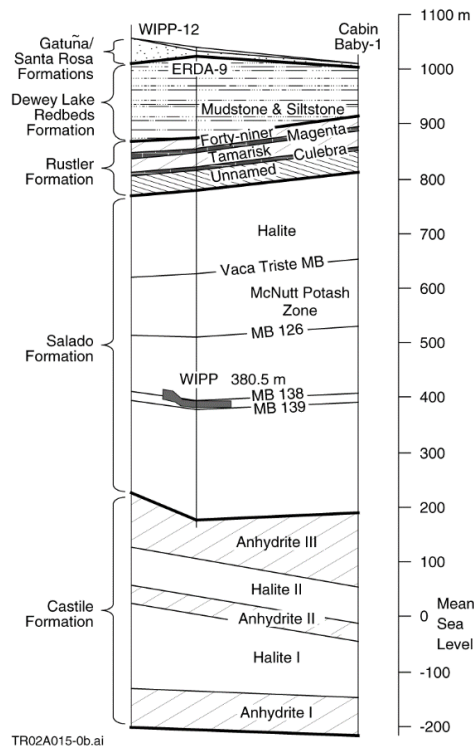


Fig. 3. Stratigraphy above and below the WIPP repository.^{1, Fig. 4; 32}

III.B.2. Salado Formation

The 600-m-thick Salado Formation, which overlays the Castile Formation, hosts the WIPP repository 654 m below the surface. Near the repository, the Salado consists of nearly horizontal ($<1^\circ$ regional dip) halite (NaCl), argillaceous halite, and occasional interbeds of clay and anhydrites (CaSO_4) of the Late Permian Period (~255 million years old or 255 Ma).^{1, Fig. 4} Farther from the repository, polyhalite layers exist ($\text{K}_2\text{Ca}_2\text{Mg}(\text{SO}_4)_4 \cdot \text{H}_2\text{O}$). The location of the room displayed in Fig. 3 is for Panels 1, 2, 7, 8, and 10. In Panels 3, 4, 5, and 6, the ceiling of the room is at clay seam G.

III.B.3. Culebra Dolomite Member of Rustler Formation

The Rustler Formation overlies the Salado. The 7.3-m thick Culebra Dolomite Member of the Rustler Formation, 216 m below the surface, is the most likely pathway for transporting radionuclides away from the repository after an inadvertent human intrusion because it is the most permeable saturated stratigraphic unit (Fig. 3).^{13; 17} The Culebra consists mostly of dolomite with minor amounts of gypsum, quartz, and clay.

The Culebra has been divided into four units near the WIPP repository, three of which are transmissive.¹³ The uppermost unit, Culebra Unit 1, averages 3.0 m in thickness but is not transmissive with only a small number of fractures that occur along bedding planes. The middle Culebra Units, 2 and 3, are similar except for the extent of fracturing. The fractures in both units typically extend less than 5 cm and connect numerous vugs. Originally, the vugs were anhydrite pockets that hydrated to gypsum during sedimentation; subsequent dissolution of gypsum left the vugs. Culebra Unit 2 is about 1.6 m thick; Culebra Unit 3 is about 1.2 m thick. The lowermost Culebra Unit 4 is typically 1.5 m thick near the repository.

III.C. Design of the Repository

The WIPP underground facility is constructed in a single stratigraphic unit of the Salado. The excavated disposal region is $4.38 \times 10^5 \text{ m}^3$. In the original design, excavated disposal region was divided into eight panels (of which 6 panels were filled as of the beginning of 2014) plus two equivalent panels composed of the 4 central connecting drifts. A full panel is $\sim 4.6 \times 10^4 \text{ m}^3$. Because of the accidental release in 2014 that contaminated some of the underground with primarily ^{241}Am , DOE plans to abandon the southern equivalent panel and closures between Panels 3, 4, 5, and 6 in the southern portion of the repository to avoid undue worker exposure. Only waste emplacement and closures for panels in the northern portion of the repository are now planned (Fig. 4).

Each panel is divided into 7 rooms. All the openings are rectangular in cross section (10 m wide, and 4 m high). Not including the connecting drifts, a room is 91.4 m long with a volume of 3642 m^3 . CH-TRU is disposed in the excavated rooms, usually in 7-packs of 55-gallon drums, stacked 3 high and 6 across the width of rooms and connecting drifts (Fig. 4).

About 5% of the remaining room volume is backfilled with bags of magnesium oxide such that the average initial porosity (including the porosity in the waste) is about 85%. Magnesium oxide (MgO) acts as a buffer to control pH of any brine that seeps into the rooms prior to waste encapsulation. The MgO also combines with any CO_2 formed during degradation of organic matter, such that highly soluble Pu carbonate species are not formed.

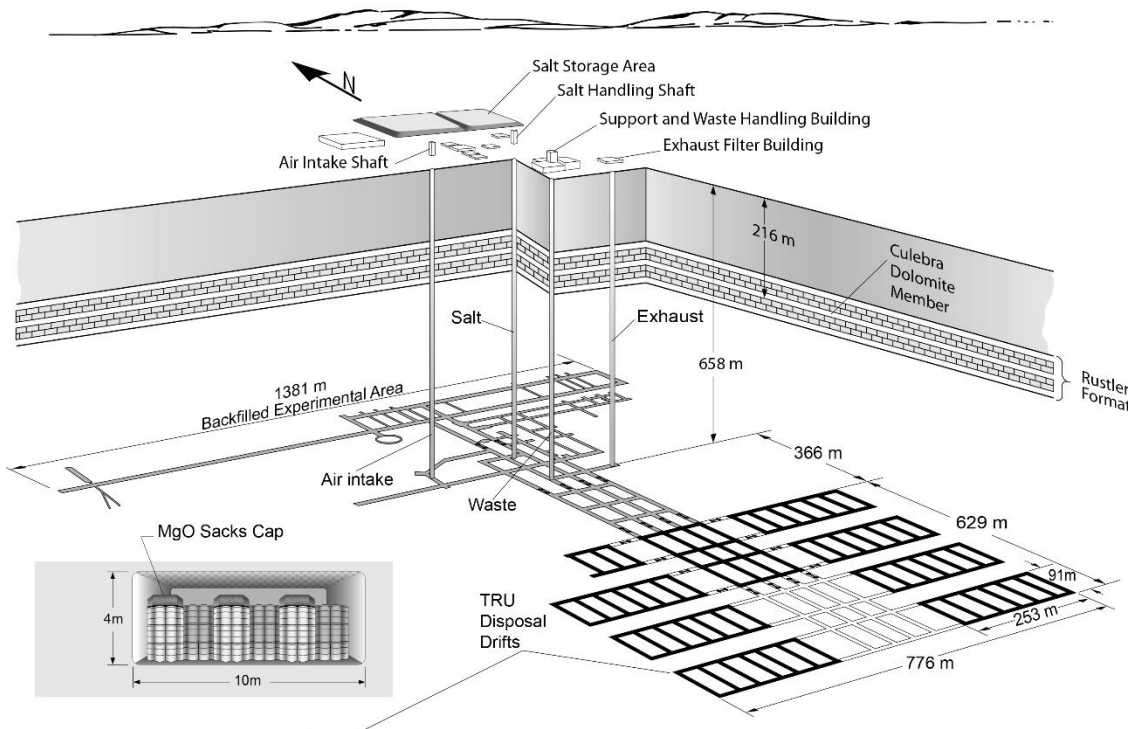


Fig. 4. The transuranic waste disposal area of the WIPP repository has 7 complete panels, an 8th partial panel, and one equivalent panel in the north central region.

IV. PLUTONIUM CONCENTRATIONS POSSIBLE AT WIPP

IV.A. Calculated Dissolved Pu Concentration

IV.A.1. Oxidation State Dependence

Actinides present in the WIPP inventory can exist in the III, IV, V, or VI oxidation states. Lower oxidation states of actinides are generally less soluble than higher oxidation states, except for Pu^{III}. Although plutonium can be present as either Pu^{III}, Pu^{IV}, Pu^V, or Pu^{VI}, or often as a combination of several of these oxidation states, the WIPP Project reasons that plutonium would exist in the lower oxidation states because of the ubiquitous presence of iron from the containers. The WIPP Project assumes that in standard waste the distribution is 50% as +3 valence (Pu^{III}) and 50% as +4 valence (Pu^{IV}).³³ The non-pit surplus Pu would be as PuO₂ at +4 valence. The WIPP Project assumes uranium would exist as either U^{IV} or U^{VI}.

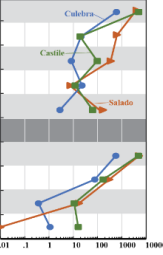
IV.A.2. pH Dependence

The pH (i.e., activity of hydronium ion [H⁺]) of the solution also influences the solubility of Pu and U. For WIPP enough MgO is placed in the repository such that any CO₂ generated by microbial degradation of organic material in the waste (e.g., paper) would form hydromagnesite, Mg₅(CO₃)₄(OH)₂•4H₂O, such that dissolved CO₂ (H₂CO₃*) would not form; thus, the pH of the brine stays within the range of 8.8 to 9.0 in the repository. Narrowing the range of pH narrows the solubility range of various radioisotopes.

IV.A.3. Brine Dependence

The range of dissolved Pu and U solubility (*S^D*) is somewhat dependent upon the ionic strength (*i*) (i.e., type of brine). Consequently, the solubility is estimated for both Salado (*i* = 6700 mM) and Castile brines (*i* = 5300 mM) in the CCA, and CRA analyses (Table II). In the solubility calculations, the composition of the Castile brine is from exploratory borehole ERDA-6.^{34; 35} The intergranular Salado brine, as measured at the repository horizon in the experimental Room Q, has substantially more magnesium, potassium, chloride, and boron than Castile brine. The Culebra brine, as measured in the Air Intake Shaft, is only slightly more saline than brackish water.^e

Table II. Composition of Castile, Salado, and Culebra brines near WIPP.³⁴

Constituent	Brine Concentration (mM or mole/m ³)			
	Culebra (Air Intake Shaft)	Salado (G - Seep)	Castile (ERDA - 6)	
Sodium (Na ⁺)	600	4110	4870	
Magnesium (Mg ²⁺)	21	630	19	
Potassium	8.3	350	97	
Calcium (Ca ²⁺)	23	7.68	12	
Boron (B ³⁺)	2.8	144	63	
Chloride (Cl ⁻)	567	5100	4800	
Sulfate (SO ₄ ⁻²)	77	303	170	
Bromine (Br ⁻)	0.37	17.1	11	
Bicarbonate (HCO ₃ ⁻¹)	1.1	0.01	16	
Ionic strength	800	6700	5300	
Total dissolved solids (kg/m ³)				
Calculated	43.2	337	305	
Measured	42.6	355	330	
Specific Gravity	1.040	1.230	1.216	
pH	7.70	6.10	6.17	

^e Herein, brine refers to an aqueous solution with total dissolved solids (TDS) greater than 30 kg/m³. For comparison, brackish water refers to solutions with TDS between 3 and 30 kg/m³. Sea water has TDS of ~35 kg/m³ and fresh water has TDS < 3 kg/m³.

IV.A.4. Baseline Actinide Solubility

The baseline solubility for an actinide oxidation state in solutions of high ionic strength, as occurs in Castile and Salado brines, was calculated using a chemical equilibrium code. For the CCA, FMT, a code specifically written for the WIPP, was used.³⁶ For CRA-2014 and CRA-2019, EQ3/6 v 8.0a was used.³⁷ Both codes accessed the WIPP database of Pitzer interaction coefficients. For CRA-2014 and CRA-2019, DATA0.FM1 version was used.³⁸ The solubility of plutonium is difficult to assess because it can readily change from either Pu^{III}, Pu^{IV}, Pu^V, or Pu^{VI}, and is often present as a combination of several of these oxidation states in experiments. However, experimental evidence suggests that actinide elements in the same oxidation state exhibit the same chemical behavior (“oxidation state analogy”),^{33; 39; 40, p.536} it was possible to use Pitzer coefficients experimentally evaluated for other actinides. Hence, Pitzer coefficients evaluated for Am^{III} were used to estimate the solubility of other III actinides such as Pu^{III}, Th^{IV} for IV actinides such as Pu^{IV}; Np^V for V actinides, and U^{VI} for VI actinides.

In CCA-1996, the solubility of both III and IV actinides (e.g., Pu^{III} and Pu^{IV}) differed substantially in Castile and Salado brines (Table III, Fig. 5). As noted CCA-1996, a Pitzer coefficient for interaction of carbonate species of IV actinides with Cl⁻¹ was unavailable at the time of submission, but was available shortly thereafter a Pitzer coefficient for Th(CO₃)₅⁻⁶ interacting with Cl⁻¹ was measured that reduced the solubility of IV actinides by 2 orders of magnitude.¹ Thus, since CRA-2004 the solubility has been similar in both brines. Furthermore, the difference between Pu^{III} and Pu^{IV} solubility has diminished.

The solubility of Pu^{III} increased substantially in both Salado and Castile brines in the CRA-2009 and CRA-2014 (Table III, Fig. 5). because complexation of actinides, such as Pu by organic ligands, especially ethylenediaminetetraacetate (EDTA), was included when evaluating actinide solubility. Actinide complexation had not been included in the CCA-1996.

Table III. Change in calculated baseline Pu and U concentration between CCA-1996, PAVT, CRA-2004, CRA-2009, CRA-2014,⁴¹ and CRA-2019 for mixing volume of 17 400 m³

Analysis	Brine	Baseline Actinide Concentrations				
		Pu ^{III} (mM)	Factor Change from CCA	Pu ^{IV} , U ^{IV} (mM)	Factor Change from CCA	U ^{VI} (mM)
CCA-1996	Salado	5.8×10 ⁻⁴		4.4×10 ⁻³		8.8×10 ⁻³
	Castile	6.5×10 ⁻⁵		6.0×10 ⁻⁶		8.7×10 ⁻³
PAVT-1997	Salado	1.2×10 ⁻⁴	0.21	1.3×10 ⁻⁵	0.003	
	Castile	1.3×10 ⁻⁵	0.20	4.1×10 ⁻⁵	6.8	
CRA-2004	Salado	3.9×10 ⁻⁴	0.67	5.6×10 ⁻⁵	0.01	1.0
	Castile	2.9×10 ⁻⁴	4.5	6.8×10 ⁻⁵	11	1.0
CRA-2009	Salado	1.7×10 ⁻³	2.9	5.6×10 ⁻⁵	0.01	1.0
	Castile	1.5×10 ⁻³	23	7.0×10 ⁻⁵	12	1.0
CRA-2014	Salado	2.6×10 ⁻³	4.5	6.0×10 ⁻⁵	0.01	1.0
	Castile	1.5×10 ⁻³	23	7.0×10 ⁻⁵	12	1.0
CRA-2019	Salado	1.6×10 ⁻⁴	0.28	5.4×10 ⁻⁵	0.01	1.0
	Castile	1.8×10 ⁻⁴	2.8	5.4×10 ⁻⁵	9	1.0
	Culebra	1.4×10 ⁻⁶		1.4×10 ⁻⁴		1.0

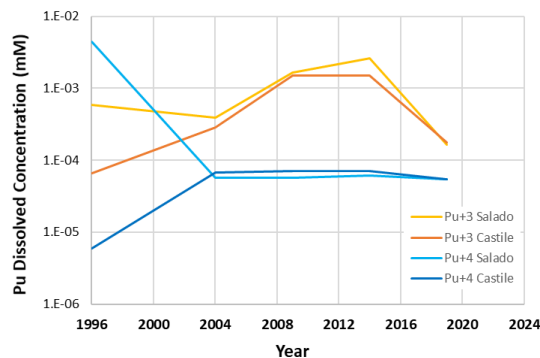


Fig. 5. Change in baseline actinide III and IV solubility in CCA-1996, CRA-2004, CRA-2009, CRA-2014, and CRA-2019.

Some competition of EDTA with metal ions in the brine (e.g., Mg^{+2}) from iron degradation was initially included, but Ca^{+2} in the Castile and Salado brines (Table II) competes strongly for EDTA, such that not much Pu^{III} -EDTA complex is formed and, thus, cannot contribute much to the total Pu^{III} solubility. Thus, the Pu^{III} solubility values have returned to values used in the CCA-1996 (Table III, Fig. 5). Because Ca^{+2} concentration is even larger in Culebra brine (Table II), organic complexation (such as EDTA) with Pu^{III} is expected to be of little importance in the Culebra and the solubility of Pu^{III} drops 2 orders of magnitude to 1.4×10^{-6} mM.

Uncertainty in Solubility. The uncertainty in solubility is potentially an important source of uncertainty in the performance measure (i.e., CCDF).¹³ Uncertainty in solubility is dependent on the uncertainty of the brine chemistry, but this chemistry is not evaluated in the CCA and CRAs. The uncertainty about the FMT and EQ3/6 calculated baseline dissolved concentration (S^{Base}) was estimated using a sampled scale factor as a function of oxidation state ($10^{f_D(Ox)}$). For CCA-1996, a piece-wise linear distribution of $f_D(Ox)$ was set by analyst judgement. The FMT calculated baseline value was set equal to the median value ($S_{50\%}^D = S_{FMT}^{Base}$). For Pu and U, the minimum was a factor of 0.01 smaller than the baseline value (i.e., $f_D = -2$ such that $S_{min,CCA}^D = 0.01 \cdot S_{FMT}^{Base}$); the maximum was a factor of 25 larger (i.e., $f_D = 1.4$ such that $S_{min,CCA}^D = 25 \cdot S_{FMT}^{Base}$).^{42,p. 5-15} Although the same distribution was used for Pu and U, the distribution was sampled separately without any correlation.

For CRA-2014, the distribution of $f_D(Ox)$ was established through comparison of a wide range of measured values and prediction from EQ3/6 for III, IV, and V actinide oxidation states. For CRA-2019, the distribution of $f_D(Ox)$ was based on an EPA requested sensitivity analysis for CRA-2014, which used a reduced set of experimental values based on 11 inclusion criteria.^f For the +III oxidation state, the minimum of $f_D(III)$ uncertainty distribution was -1.14 . Hence the minimum was a factor of 0.07 (i.e., $10^{-1.14}$) smaller than the EQ3/6 calculated value (i.e., $S_{min,CRA19}^D = 0.07 \cdot S_{EQ3/6}^{Base}$); the maximum was a factor of 933 (i.e., $10^{2.97}$) larger (i.e., $S_{max,CRA19}^D = 933 \cdot S_{EQ3/6}^{Base} = 1.7 \times 10^{-1}$ mM in Castile brine). The

^f The 11 criteria specified inclusion of results from only studies⁴³ (1) published between 1990 and 2011; (2) published in journals and official government laboratory reports; (3) of solubility (not corrosion, sorption, etc.), (4) with water as solvent; (5) near atmospheric pressure and WIPP temperatures—20 to 30 °C; (6) of Th^{IV} , Nd^{III} , Am^{III} , and Cm^{III} , not studies of U^{IV} , Np^{IV} , Pu^{III} , and Pu^{IV} because of difficulty in maintaining oxidation state of U, Np, Pu; (7) with controlling solid in WIPP certified thermodynamic database; (8) with known aqueous composition, not general studies in groundwater, etc; (9) with dissolved species in WIPP certified thermodynamic database; (10) with complete description of experiments, not studies summarized in literature reviews; and (11) with conditions similar to WIPP, that is, ionic strength ≥ 3000 mM, total inorganic carbon ≤ 14 mM, and $8 \leq pH \leq 11.2$.

mean and median were $10^{0.640} = 4.37$ and $10^{0.345} = 2.21$ respectively, times the EQ3/6 calculated value. For the IV oxidation, the minimum factor was $10^{-2.0} = 0.01$ and the maximum factor was $10^{1.43} = 27$ (i.e., $S_{\max, CRA19}^D = 27 \cdot S_{EQ3/6}^{Base} = 1.5 \times 10^{-3}$ mM in Castile and Salado brines), which is like the uncertainty distribution for the CCA-1996. The mean and median were $10^{-0.00486} = 0.99$ and $10^{-0.0996} = 0.80$, respectively.

Table IV. Uncertainty factors about calculated baseline dissolved concentration for +III and +IV actinide oxidation states in CCA-1996, CRA-2014, and CRA-2019

Analysis	Actinide Oxidation	Mean ($10^{f_{mean}^D}$)	Median ($10^{f_{median}^D}$)	Minimum ($10^{f_{min}^D}$)	Maximum ($10^{f_{max}^D}$)
CCA-1996	Pu ^{III} , Pu ^{IV} , U ^{IV}		1.0	0.01	25
CRA-2014	Pu ^{III}	0.21	0.13	0.0003	933
	Pu ^{IV} , U ^{IV}	4.71	10.70	0.03	1550
CRA-2019	Pu ^{III}	4.37	2.21	0.07	933
	Pu ^{IV} , U ^{IV}	0.99	0.80	0.01	27

IV.B. Calculated Colloidal Concentrations

Four categories of colloids are considered at WIPP: mineral, intrinsic, humic, and microbial.³⁵ The mineral-type colloids are mineral substrates that readily adsorb actinides; the intrinsic colloids are polymeric radioisotopes; the microbial colloids are microbes that have adsorbed actinides; and the humic colloids are actinides complexed by humic organics. The mineral colloid concentration ($C^{mineral}$) was fixed at 2.6×10^{-5} mM.⁴⁴ Only Pu was assumed to form intrinsic colloids at a fixed concentration (C^{int}) of 4.3×10^{-5} mM.⁴⁵ The concentration of humic colloids was assumed to be a fraction of the dissolved concentration (S^D), where the fraction was a function of the ionic strength (or brine type [Br]), oxidation state (Qx), and radioisotope (Rn) (i.e., $C^{humic} = f^{humic}(Br, Ox, Rn) \cdot S_D$). The humic colloidal concentration was assumed to be bounded by 0.011 mM.⁴⁶ Experiments with WIPP-relevant microbes found that microbes do not actively move actinides through the cell membrane, but instead passively adsorb actinides extracellularly similar to mineral adsorption.⁴⁷ Hence, the microbial colloidal concentration was also a function of brine type, oxidation state, and the radioisotope.

IV.C. Calculated Total Pu Concentration

A total concentration of Pu was calculated as the sum of the dissolved species (S_D) and the four categories of colloids.^{33, Table I; 48, Table SOTERM-21}

$$C_{Pu}^T = 10^{f^D} S_{EQ3/6}^D + C^{humic} + C^{microbe} + C^{mineral} + C^{int} \quad (17)$$

where

$$C^{humic} = \min \{ 10^{f^D} S_{EQ3/6}^D f^{humic}, 1.1 \times 10^{-2} \text{ mM} \}$$

$$C^{microbe(III)} = \min \{ 10^{f^D} S_{EQ3/6}^D f^{microbe}, 2.3 \times 10^{-6} \text{ mM} \}$$

$$C^{microbe(IV)} = \min \{ 10^{f^D} S_{EQ3/6}^D f^{microbe}, 3.8 \times 10^{-5} \text{ mM} \}$$

$$C^{mineral} = 2.6 \times 10^{-5} \text{ mM}$$

$$C^{int}(Pu) = 4.3 \times 10^{-5} \text{ mM}$$

Table V. Total Concentration of Pu in Salado and Castile Brines in CRA-2019.

	Baseline ($S_{EQ3/6}^{Base}$) (mM)	Factor ($10^{f_{mean}^D}$)	Dissolved (S_{mean}^D) (mM)	Colloids				Total Concentration (C ^T) (mM)	Fraction Colloid	Filterable Colloid Fraction (Microbe Mineral)
				Humic Scale Factor f_{humic}^D	Microbe Scale Factor $f_{microbe}^D$	Mineral $C_{mineral}^{int}$ (mM)	Intrinsic C^{int} (mM)			
<i>Salado Brine with Mean Uncertainty Factor</i>										
Pu ^{III}	1.6×10^{-4}	4.37	7.0×10^{-4}	0.20	0.03	2.6×10^{-5}	4.3×10^{-5}	9.1×10^{-4}	0.23	0.03
Pu ^{IV}	5.4×10^{-5}	0.99	5.3×10^{-5}	0.01	0.21	2.6×10^{-5}	4.3×10^{-5}	1.3×10^{-4}	0.60	0.28
<i>Salado Brine with Maximum Uncertainty Factor</i>										
Pu ^{III}	1.6×10^{-4}	933	1.5×10^{-1}	0.20	0.03	2.6×10^{-5}	4.3×10^{-5}	1.8×10^{-1}	0.17	0.00
Pu ^{IV}	5.4×10^{-5}	27	1.5×10^{-3}	0.01	0.21	2.6×10^{-5}	4.3×10^{-5}	1.6×10^{-3}	0.08	0.04
<i>Castile Brine with Mean Uncertainty Factor</i>										
Pu ^{III}	1.8×10^{-4}	4.37	7.9×10^{-4}	0.20	0.03	2.6×10^{-5}	4.3×10^{-5}	1.1×10^{-3}	0.23	0.03
Pu ^{IV}	5.4×10^{-5}	0.99	5.3×10^{-5}	0.01	0.21	2.6×10^{-5}	4.3×10^{-5}	1.3×10^{-4}	0.60	0.28
<i>Castile Brine with Maximum Uncertainty Factor</i>										
Pu ^{III}	1.8×10^{-4}	933	1.7×10^{-1}	0.20	0.03	2.6×10^{-5}	4.3×10^{-5}	2.0×10^{-1}	0.17	0.00
Pu ^{IV}	5.4×10^{-5}	27	1.5×10^{-3}	0.01	0.21	2.6×10^{-5}	4.3×10^{-5}	1.6×10^{-3}	0.08	0.04

IV.D. Calculated Pu Adsorption

For modeling, adsorption in geologic media is most often expressed as the ratio of mobile material (here, the mobile U and Pu in the brine) and material on the immobile rock (here, corrosion products in the repository or dolomite in the Culebra).^g The distribution coefficient (K^D) in the Freundlich isotherm model is defined^{40, p. 353}

$$\frac{x_r}{m^s} = K^D (C^e)^\lambda \quad (18)$$

where x_r is mass of attached adsorbate radionuclide r on the solid, m^s is the mass of immobile solid, C^e is the equilibrium concentration of the adsorbate in the solution, and λ is a number > 0 .

If the WIPP repository is somewhat oxidizing, the initial iron corrosion products of the steel within the WIPP repository may be nanoparticles of amorphous ferrihydrite (i.e., Fe^{+3}). The amorphous ferrihydrite (nominally $5Fe_2O_3 \cdot 9H_2O$ though the formula varies with water content) may progress, through dehydration and aggregation, to more crystalline goethite (α - $FeO(OH)$),^h or hematite (α - Fe_2O_3),⁵⁰ provided metal cations readily absorbed on ferrihydrite do not block the transformation.⁵¹ Ferrihydrite is rapidly catalyzed by Fe^{+2} to form goethite.⁴⁹ Transformation of ferrihydrite to hematite can take longer.

Because ferrihydrite has an indeterminate formula and hematite is less adsorptive, we assume the iron corrosion product is goethite. Isotherms of Pu^{IV} and Pu^V adsorption on goethite at high solution concentrations of plutonium have $K_{rust, Pu}^D$ of 0.21 mole Pu/kg rust and λ if 0.72.^{1, Fig. 17b}

^gHerein, adsorption refers to the accumulation of material at the interface of another material. Adsorption subsumes several different mechanisms (e.g., surface complexation and ion exchange). Because geochemical adsorption is not strictly a surface phenomenon, some geochemists prefer to use the more inclusive term "sorption." However, this article uses the more traditional terms adsorption and absorption, with the latter used when referring to neutron absorption (capture) by the nucleus.

^h Lepidocrocite (γ - $FeO(OH)$), a polymorph with different crystal structure is favored in chloride solutions,⁴⁹ but adsorption data are less readily available.

If the repository is very reduced, then goethite is not formed since Fe^{+3} is not present. Instead, an $\text{Fe}(\text{OH})_2$ iron hydroxide (i.e., Fe^{+2}) would form. Because of the great difficulty in maintaining a reducing solution of Pu^{III} , adsorption of Pu^{III} on $\text{Fe}(\text{OH})_2$ has not been measured.

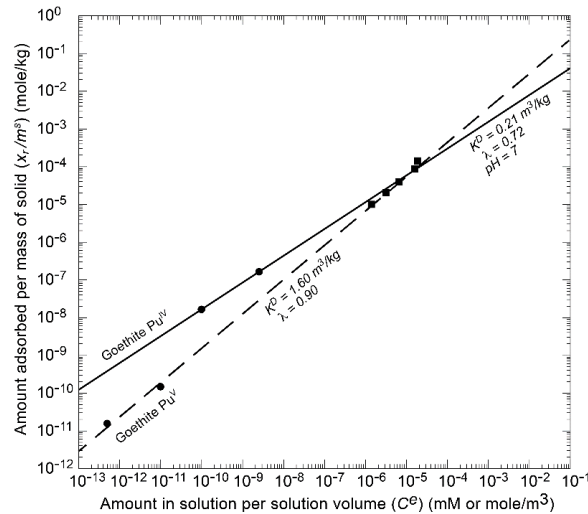


Fig. 6. Adsorption of Pu^{IV} and Pu^{V} on iron oxides at neutral pH in water (dots)⁵² and J-13 well water (squares)¹. Fig. 17b; 53

IV.E. Fissile Critical Mass and Concentration in Mixtures of Brine and Geologic Media

The criticality limits used herein are based on modeling mixtures of water, salt, dolomite, concrete, rust, and fissile material using a neutron/photon transport computational code. In a companion report,⁵ several idealized depositional spheres of fissile material homogeneously mixed with fluids and the host rock were analyzed. Substituting WIPP brines for water substantially increases the mass of fissile material necessary to go critical for both ^{239}Pu and ^{235}U . The addition of geologic media to a fissile/water binary system also substantially increases the mass of fissile material necessary to go critical (Table VI).

The influence of geologic media in an infinite mixture on the limiting concentration varies. For geologic material primarily composed of absorbing elements such as iron in rust or chloride in salt, the geologic material increases the critical concentration compared to fissile/water binary system. For geologic material primarily composed of weak moderators such as silicon, it often decreases the critical concentration (Table VI).

The porosity of the geologic media has a strong influence on both the critical mass and the critical concentration in Culebra brine (and H_2O). As the porosity increases, the behavior approaches that of a fissile/fluid binary system and greatly decreases the critical mass (Fig. 7)

Media heterogeneity is somewhat influential on the minimum critical mass of sphere (Fig. 7) but less so on the minimum critical concentration of an infinite mixture with Culebra dolomite (Fig. 8). Hence, heterogeneity is important when deposition only occurs in a portion of the porosity (here the fracture porosity) and the total porosity is small, even at high enrichment.

Table VI. Minimum concentration for infinite mixture and minimum mass and concentration for reflected sphere of Pu and U mixed homogeneously with WIPP brine and Culebra dolomite, concrete, goethite, and salt materials at 20% porosity.⁵

Fluid	Solid Material	Infinite Mixture Min Concen (kg/m ³)	Reflected Sphere		
			Mass Min (kg)	Radius Min (m)	Concen at Min mass
Plutonium 100% enriched					
Water	none	7.2	0.50	0.16	32
	Culebra Dolomite	2.9	1.8	0.31	14
	Goethite (FeO(OH))	19	3.0	0.22	79
Culebra	none	11	0.80	0.15	54
	Culebra Dolomite	3.7	2.3	0.33	15
Castile	none	40	3.8	0.18	160
	Culebra Dolomite	9.8	7.5	0.37	35
	Goethite	25	4.3	0.23	89
Salado	none	52	5.0	0.19	190
	Culebra Dolomite	12	9.7	0.38	42
	Salt (NaCl)	180	150	0.26	2000
	NRC Concrete	13	6.0	0.31	49
	Goethite	27	4.8	0.23	100
Uranium 5% enriched					
Water	none	300	32	0.19	1070
Culebra	none	470	69	0.22	1600
	Culebra Dolomite	180	435	0.63	420
Salado	none	2800	2300	0.44	6200

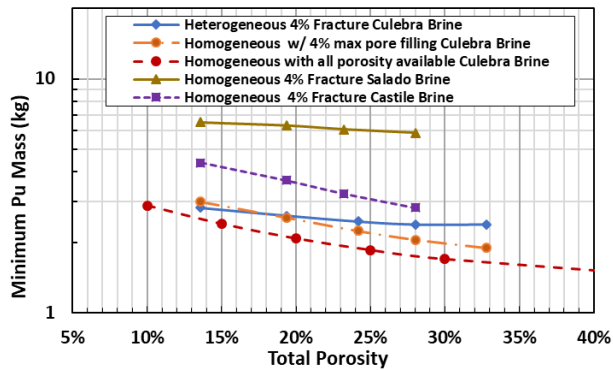


Fig. 7. Critical Pu mass for homogeneous models less than for heterogeneous model with total porosity >18% and 4% fracture porosity in Culebra dolomite.⁵

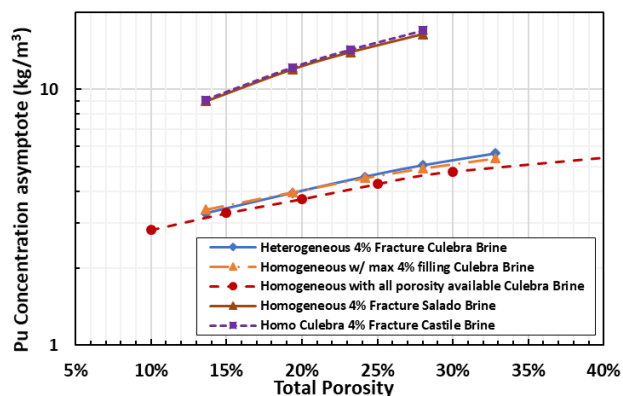


Fig. 8. Minimum critical concentration for a mixture of infinite extent influenced by total porosity and pore fluid type but not media heterogeneity in Culebra dolomite.⁵

V. LACK OF CRITICALITY POTENTIAL PRIOR TO INADVERTENT INTRUSION

V.A. Hydrologic Constraint on Brine Movement

Possible hydrologic mechanisms to move critical masses of the fissile material to more favorable locations within the repository do not exist. Prior to a hypothetical human intrusion, on average $29.8 \times 10^3 \text{ m}^3$ of brine flows *into* the repository through the ubiquitous disturbed rock zone (DRZ) and anhydrite layers in CRA-2019 (Scenario S1-BF in Table VII). An intrusion somewhat increases the average influx since it can relieve gas pressure (Scenario S4-BF) but an intrusion into a hypothetical underlying brine pocket (Scenario S2-BF or S6-BF) is required to substantially increase brine influx (Table VII). Furthermore, an intrusion into a brine pocket is required to get substantial brine flow up the intrusion borehole and fissile release into the Culebra dolomite.

Table VII. Mean cumulative brine flow into repository and up intrusion borehole in CRA-2019.

Brine Flow Location	Scenario ^a	Brine Flow	
		Mean ^b (m^3)	Max (m^3)
Into Repository			
No Intrusion	S1-BF	29.8×10^3	31.8×10^3
Castile Pocket Intrusion	S2-BF	100.0×10^3	112.0×10^3
Repository only Intrusion	S4-BF	30.6×10^3	37.8×10^3
Repository and Castile Pocket Intrusion	S6-BF	60.0×10^3	75.8×10^3
Up Intrusion Borehole			
	S2-BF	4.72×10^3	7.54×10^3
	S4-BF	0.096×10^3	0.86×10^3
	S6-BF	4.17×10^3	7.53×10^3

^aSee Table VIII

^bMean of all 3 replicates (300 samples)

The brine flows diminish as the DRZ heals and the repository pressurizes somewhat from gases produced by the anoxic corrosion of steels and microbial degradation of organic material such as plastics in the waste. The brine is sometimes completely consumed by the anoxic corrosion process, in which case, no long-term gradient exists for brine movement through repository whereby fissile material can be moved.

In those cases, where sufficient brine seepage occurs, the limited hydraulic gradient from the 1% dip of strata could allow Pu disposed in northern panels to migrate into southern panels. However, the migration is from containers with high fissile mass, in the case of POCs (and CCOs), to generally low fissile mass. More importantly, geochemical constraints are not favorable for concentrating fissile material in the WIPP waste disposal rooms through high solubility, sorption, and precipitation, as discussed below (§V.C).

V.B. Geochemical Constraints

V.B.1. Dissolved Concentration

The maximum dissolved $^{239}\text{Pu}^{\text{III}}$ concentration of 0.17 mM in Castile brine in CRA-2019 (i.e., $10^{f_D} \cdot S_{EQ/6, \text{Pu}^{239}}^{\text{Base}} = 933 \cdot 1.8 \times 10^{-4}$ mM—Table V) is 3 orders of magnitude below the limit necessary to create a critical solution of ^{239}Pu in Castile brine (i.e., 0.17 mM or 0.04 kg/m^3 versus 40 kg/m^3 —Table VI). The maximum dissolved $^{239}\text{Pu}^{\text{IV}}$ concentration of 0.0015 mM in either Castile or Salado brine is 5 orders of magnitude below the limit necessary to create a critical solution in Castile brine (0.0015 mM or $3.5 \times 10^{-4} \text{ kg/m}^3$ versus 40 kg/m^3).

A similar situation exists for ^{235}U , the other primary fissile radionuclide. The maximum dissolved U^{VI} solubility of 1 mM (0.235 kg/m^3) without uncertainty (as specified by EPA since CRA-2004) is 3 orders of magnitude lower than a critical solution of 5% enriched U in pure water, (i.e., 300 kg/m^3 —Table VI).

V.B.2. Precipitation

A fairly uniform material distribution implies that the geochemistry is fairly uniform without local variation in pH, ionic strength, or reduction-oxidation potential to promote preferential precipitation. For example, there is little chance of great variation in the redox state of the brine from one place to another, because Fe^0 iron is present throughout the waste. To elaborate, the main determinant of oxidation states within the repository will be the rate of interaction with elemental iron, Fe^0 , and the rate of microbial-facilitated reduction of oxidized species, such as nitrate and sulfate. The resulting repository brines are expected to have relatively high concentrations of reducing species such as Fe^{II} and S^{II} . Hence, the most likely states are Pu^{III} and Pu^{IV} and not higher oxidation states of Pu^{V} and Pu^{VI} . Surplus non-pit Pu will be disposed as PuO_2 (Pu^{IV}), and reduction of Pu^{IV} to Pu^{III} would increase the solubility of Pu, not decrease it (Table III).

V.B.3. Geochemical Constraint on Adsorption in Repository

Within the WIPP repository, conditions that might lead to potential adsorption of Pu or U on corrosion products in a localized area do not exist. Granted, the waste from each storage/generation site contains a wide variety of potentially adsorptive material, such as soils, waste solidifiers (e.g., bentonite clay), corroded metals, and degraded glass; however, the potentially adsorptive waste materials are not concentrated in a few drums. Rather, adsorptive materials are fairly uniformly distributed throughout the repository and preferential concentration of plutonium in one area is unlikely. Similarly, substrates and nutrients for biofilms that might cause fissile concentration are also disseminated fairly uniformly throughout the repository.

Furthermore, a difficulty in proposing adsorptive backfill as an engineered barrier in the WIPP repository is that the adsorption on proposed backfills is not specific and so large amounts of other material that are in the waste also adsorb. This situation decreases the likelihood of criticality because many of these materials (e.g., nonfissile actinides, iron, nickel, and lead) readily absorb neutrons and prevent a critical excursion.

V.B.4. Limits on Dispersed Colloidal Concentration

The concern with colloids is (1) whether the concentration of colloids is critical or (2) whether there is a mechanism by which actinide-bearing colloidal particles can be locally concentrated through aggregation or filtration. Similar to adsorption, the uptake of fissile actinides by the various types of colloidal particles is governed by equilibrium among dissolved actinides, solid actinide phases, and the colloidal particles. The link between colloidal actinide concentration and equilibrium thermodynamics produces a limit on the concentration of colloidal actinides that cannot reasonably exceed by 2 orders of magnitude the fissile dissolved concentration and thereby go critical.

V.B.5. Fate of Colloids in Repository prior to Intrusion

The behavior of the colloidal particles themselves is best described as a steady-state process, in which new particles are continuously generated and dispersed in the liquid phase but are gradually destabilized through a variety of processes. Destabilization of mobile colloidal fissile actinides, followed primarily by gravitational settling, could conceivably concentrate fissile material, but the mechanism is limited to local microenvironments that are likely to be centimeter-sized or even smaller within the WIPP repository. After closure of the repository, salt creep will crush the waste containers and compact waste material. Colloidal particles could form throughout the waste matrix; however, the fluid columns in which agglomerated colloidal particles will settle are likely to be short and poorly connected. Consequently, the local concentrations of colloidal agglomerates that develop in the WIPP will remain uniformly distributed in the waste throughout the repository and will not concentrate in a single location. By analogy to a closed house, dust (i.e., aerosols) settles on the horizontal surfaces in the house. The dust does not concentrate at a single location.

VI. LACK OF CRITICALITY POTENTIAL IN DISPOSAL AREA AFTER INTRUSION

VI.A. Geochemical Constraint on Precipitation in Disposal Area

After inadvertent human intrusion, gas pressure can be released and allow more brine to enter the repository. Like the situation prior to intrusion, however, a fairly uniform material distribution implies that the geochemistry is fairly uniform without local variation in pH, ionic strength, or reduction-oxidation potential to promote preferential precipitation.

After inadvertent human intrusion into a hypothetical brine pocket below the repository, more brine can flow into the repository (mean factor of 2.5 more brine after intrusion into hypothetical brine pocket—Table VII).^{20, Table 4-5} However, the Castile brine in the repository does not substantially change the solubility of the Pu either in the +III or +IV oxidation state (i.e., the solubility is of the same order of magnitude—Fig. 5). Hence, the Castile brine does not introduce a geochemical situation for precipitation within the repository.

VI.B. Geochemical Constraint on Adsorption in Repository

The same general conditions preventing criticality in the repository are the same before and after an inadvertent intrusion: (1) adsorptive substrates are uniformly spread throughout the repository and not concentrated in repository sub-regions and (2) adsorption not exclusive to fissile material; readily available metal cations in the seeping brine such as Ca^{+2} and Mg^{+2} compete for adsorptive sites. Even in microenvironments, adsorption does not typically produce critical concentrations.

For Pu^{IV} (or even Pu^{III}) adsorption on goethite, the mean concentration is much less than the minimum critical concentration of 26 kg/m^3 for a mixture of goethite and Pu in Salado brine (Table VI)). That is, for the mean solubility

concentration of 5.3×10^{-5} mM (Table V), Pu^{IV} adsorption on goethite (x/m), assuming the non-linear isotherm for Pu^{IV} of §VI, is 1.8×10^{-4} mole Pu/kg goethite, which is equivalent to 0.11 kg/m^3 (i.e., $\frac{x}{m} M_{\text{Pu}}^{\text{weight}} \rho_{\text{rust}}^{\text{density}} (1 - \phi_{\text{rust}})$ where $\rho_{\text{rust}}^{\text{density}}$ is 3300 kg/m^3 and ϕ_{rust} is 20%). The 0.11 kg/m^3 is a factor of 240 less than the minimum critical concentration of 26 kg/m^3 .

Furthermore, adsorption on goethite at the maximum concentration of Pu^{IV} is also much less than the minimum critical concentration of 26 kg/m^3 (Table VI). That is, for a maximum Pu^{IV} concentration of 1.5×10^{-3} mM (Table V), the adsorption on rust is equivalent to 1.2 kg/m^3 or a factor of 22 less than the minimum critical concentration of 26 kg/m^3 . Even then, these calculations assume no competition from other cations such as Ca^{+2} and Mg^{+2} and a neutral pH of 7. The brine pH is near 9, when buffered by MgO, and the brine has high concentrations of Ca^{+2} and Mg^{+2} , which compete for adsorption sites; both situations reduce adsorption.ⁱ

VI.C. Geochemical Constraint on Colloidal Filtration after Intrusion

In a disturbed repository, flowing brine could result in filtration of any dispersed colloidal actinides, but concentration of colloidal actinides will again be localized in small microenvironments. As described above, the waste will contain many centimeter-sized microenvironments of small poorly connected pores. Filtration can take place in interstices at the boundaries of marked changes in pore size, resulting in small concentrations of colloidal actinides in those localized small areas.

Again, considering the dusty-house analogue, an air stream flowing through an open house is similar in concept to brine flowing through the repository. In the dusty house, dust that has settled on horizontal surfaces is stirred up and concentrated in local environments, such as corners or other areas where horizontal air velocity is small. In the repository, local accumulations will develop in a similar fashion. However, the tight packing of the waste will provide local filtration of colloidal particles. Hence, the fissile actinides associated with colloidal particles will remain fairly uniformly distributed within the repository on a macroscopic scale.^j

VII. LACK OF CRITICALITY POTENTIAL IN GEOLOGIC SYSTEM AFTER INTRUSION

VII.A. Lack of Favorable Depositional Features in Geologic System of WIPP

VII.A.1. Geometric Constraint on Depositional Space in Anhydrite Layers and Boreholes Near Repository

Anhydrite layers within 20 m of the repository horizon, have insufficient thickness to contain a 0.5-m diameter sphere of ^{239}Pu in salt (Fig. 3: MB 140, .08 m thick; Anhydrite “a”, 0.21 m thick; and MB 138, 0.19 m thick). The only exception is the ~0.9-m thick Marker Bed (MB) 139 directly below the repository. In MB 139, hydrologic conditions do not favor substantial movement of brine carrying dissolved Pu, as noted in §VII.A.2 below. Furthermore, geochemical conditions do not favor deposition, as noted in §VII.A.3 below

ⁱ The existence of much Pu^{III} in the repository would imply the existence of much Fe^0 and Fe^{+2} to reduce Pu^{IV} and, thus, not much ferrihydrite or goethite. Hence, using the maximum solubility of Pu^{III} (Table VI) with an extreme uncertainty factor of 933 (Table VII) in the Freundlich model for Pu^{IV} is not appropriate for Pu^{III} .

^j The minimum Pu mass for criticality provides a rough sense of the macroscopic scale in WIPP. Assuming precipitation/adsorption around Fe or Fe colloidal aggregation, the minimum ^{239}Pu mass is 5.1 kg (Table VI). For standard waste with 0.325 kg FME per 14 drums in TRUPACT-II transport cask, requires 220 drums (i.e., many standard containers are required to collect enough fissile Pu). Less containers are required for POCs and CCOs: 25.5 POCs at the maximum 0.2 kg FME per drum in TRUPACT-II and 15.7 CCO at the maximum 0.325 kg FME per drum in TRUPACT-II. For POCs in Panel 1, Room 3 with an average 0.14 kg FME, 36.5 containers are required.⁷

Similarly, intrusion boreholes do not have sufficient space to contain a sphere of ^{239}Pu . At the Culebra horizon, oil and gas wells are using 16 ¼ in (0.413 m) and 17 ½ in (0.444 m) diameter casing. At the repository horizon, oil and gas wells are using 12 ¼ in (0.31 m) and 14 in (0.356 m) casing. To have sufficient space to have criticality and avoid excessive neutron leakage, a borehole filled with salt and brine requires a diameter of 0.5 m; a borehole filled with fractured NRC concrete, requires a diameter of 0.62 m; a borehole filled with Culebra dolomite and Culebra brine requires a diameter of 0.66 m (Table VI).

VII.A.2. Hydrologic Constraint on Depositional Location in Culebra

Because of its higher permeability relative to other strata in the area (other anhydrite layers in the Salado, or layers in the Rustler formation), any dissolved radioisotopes released from the repository through the intrusion borehole enter the Culebra dolomite strata in the hypothetical simulations. Yet, the probability of criticality is low in the generally inhospitable Culebra. Absent any special circumstance for concentrating fissile material, the general tendency is for fissile material entering the Culebra to disperse because of hydrologic conditions. Hence the most likely area to reach a critical concentration through precipitation, adsorption, or colloid aggregation/filtration of colloids is near the intrusion borehole.

Furthermore, in order to agree with the observed varying salinity in the Culebra saturated zone,^{54; 55} formations above must slightly recharge the Culebra rather than Culebra fluid leak into other formations in regional groundwater models. Hence, deposition will not tend to occur in adjacent formations.

VII.A.3. Unfavorable Conditions for Precipitation in Culebra

The fissile material solution must be greatly concentrated from its repository concentration in CRA-2019 to form a critical concentration in the Culebra saturated zone. Yet, like the disposal area, several unfavorable geochemical conditions exist to prevent criticality within the geologic system from precipitation, adsorption, and colloidal filtration. The necessary condition for precipitation of fissile material and other major components of the brine is a change in the brine chemistry, which includes the redox state and buffer capacity, pH, ionic strength, or solute concentrations, such that the solubility of a component is reduced.

Change in Redox State. The traditional mechanism of forming uranium ore bodies through precipitation by reduction of a more soluble high-oxidation-state actinides cannot occur because the fissile material will be reduced within the repository. Two hypothetical scenarios of precipitation from oxidation seem unlikely: (a) the oxidation of Pu^{III} to less soluble Pu^{IV} as it is removed from the Fe^0 in the repository and (b) the oxidation of Fe^{II} to Fe^{III} , adsorption of Pu on the amorphous ferrihydrite ($\text{am-5Fe}_2\text{O}_3 \bullet 9\text{H}_2\text{O}$) and coprecipitation with Pu. Specifically, the Culebra brine and dolomite have low concentrations of active oxidation (or reduction) species. Also, a strong oxidant (or a strong reductant) in a localized area has not been discovered within the Culebra. Furthermore, the availability of sufficient oxygen from the surface through a degraded plug with the permeability of silty sand is unlikely. Consequently, a substantial change in the redox state (Eh) of the brine as it moves through the Culebra is unlikely. Any precipitation or coprecipitation that might occur would be gradual and diffuse over an area too large to cause criticality.

Carbonate Rich Brine. Uranium ores in sedimentary rocks other than sandstone are uncommon in the United States (<5%). Conditions for the deposition of uranium in carbonate rocks, such as limestone or dolomite, are

especially unfavorable because carbonate complexes are highly soluble^k hence, carbonate rocks typically contain no more than 1 ppm uranium.⁵⁶

Plutonium carbonates are also highly soluble, just not as soluble as uranium carbonates. Thus, conditions for deposition of plutonium in the Culebra dolomite is unfavorable. Just as important, formations above and below the Culebra also do not have complexing agents such as vanadium or indigenous reductants/oxidants.

VII.A.4. Geochemical Constraint on Adsorption in Culebra

Criticality is unlikely for Pu adsorption on dolomite. To elaborate, the density of adsorption sites on dolomite would have to be very large, especially, since surface complexation at adsorption sites would not be limited to ²³⁹Pu. Adsorption experiments for radioisotopes at high concentrations are difficult for evaporates and have not been done for dolomite. Brady et al.³⁹ report that if all the Mg⁺² and Ca⁺² ions present in a layer of dolomite were available for ion exchange, the maximum density would be 30 sites/nm²; however, not all Mg⁺² and Ca⁺² ions are available and so the site density is probably much lower. Hence, a bounding estimate of the required adsorption site (through ion exchange), and thus the maximum amount of fissile material that can adsorb onto a small volume, was made for dolomite and compared to other highly adsorptive natural materials.

The measured mass-specific surface area on carefully crushed and lightly acid-washed samples of dolomite from the WIPP Air Intake Shaft, as evaluated by Brunauer-Emmett-Teller (BET) surface area analysis, varies from 500 m³/kg for indurated dolomite to 2600 m³/kg for silty dolomite;^{57, App. C} these values correspond to between 1×10^6 and 6×10^6 m² of surface area per m³ of dolomite (assuming an available porosity of 16% and dolomite grain density of 2820 kg/m³). The critical Pu concentration of 3.7 kg/m³ (Table VI) corresponds to 7.6×10^{24} atoms/m² of dolomite. Dividing this critical Pu concentration (which is assumed absorbed on the dolomite surface) by volume-specific surface area requires a site density of between 1 and 7 atoms/nm². This range is similar to the observed site density for many highly adsorptive natural minerals (~2 sites/nm²).⁵⁸

Thus, obtaining a critical concentration requires the entire capacity of a highly adsorptive natural material (of which Culebra dolomite is reasonably bound). Furthermore, ²³⁹Pu would be competing with other radioisotopes and metal cations in the brine (e.g., Ca⁺² and Mg⁺²) to dislodge already adsorbed material present on the dolomite. Consequently, adsorption, by itself, is an unlikely mechanism for concentrating massive amounts of fissile material in a small area to obtain a critical solid concentration because of limitations in the adsorptive surface area available in natural geologic systems.¹

^kUnder some circumstances, uranium is associated with carbonate rocks. A small uranium ore deposit of the Jurassic Period occurs near Grants, New Mexico, the Entrada Sandstone aquifer, is overlain by the Todilto Limestone Formation (like dolomite but lacking Mg). A highly fractured area allowed water carrying uranium to move into the limestone and deposit uranium in the presence of H₂S.¹ In addition, of the three main types of vein deposits in the Schlemma uranium field of the western Ore Mountains of Germany (the largest vein-style uranium deposit in the world), one vein type consists of uraninite and dolomite formed when uranium in the area was remobilized and deposited under reducing conditions (~170 Ma).¹ In a dual porosity formulation, retardation of Pu occurs because of (1) chemical adsorption on the fracture flow surfaces (chemical retardation), and (2) diffusion into the pores of the matrix (physical retardation). Physical retardation is an important mechanism in that much of the Pu released to the Culebra does not reach the Land Withdrawal Boundary (Fig. 1). The Pu diffusing into the brine filled pores does not deposit and fill the pores as occurs with precipitation; rather, the pore fluid concentration approaches the Pu fracture concentration. The criticality limits of §IV are not noticeably influenced by the small additional amount of Pu dissolved in the matrix pore fluid; none-the-less, the limits reported here (e.g., 3 kg/m³) include dissolved fissile material in the pores and fractures.

VII.A.5. Regulatory Constraint at Disposal System Boundary

The Individual Protection Requirement in 40 CFR 191 at the accessible environment 0.15 mSv/yr is ~ 78 pCi/L for ^{235}U or ~ 5.5 pCi/L for ^{239}Pu .^m In turn, the 5.6 pCi/L is $\sim 4 \times 10^{-10}$ mM for ^{239}Pu ,ⁿ which is 11 orders of magnitude less than that required to go critical (i.e., 4.6 mM or 11 kg/m³—Table VI). The Ground Water Requirement in 40 CFR 191 at the accessible environment is more stringent for ^{235}U —15 pCi/L. The equivalent radioisotope concentrations of 15 pCi/L for ^{235}U is 3×10^{-5} mM, which is 8 orders of magnitude less than required to go critical (i.e., 1300 mM or 300 kg/m³ in pure water—Table VI). Hence, if the Individual Protection Requirement and Ground Water Requirements are met, there is insufficient concentration to cause criticality near the boundary of the accessible environment

VII.B. Modeling of Fissile Release to Culebra

In addition to the generally unfavorable geochemical conditions for criticality discussed in the previous sections, the results of the CRA-2019 analysis confirm that conditions at WIPP are not conducive to criticality.

VI.B.1. Pu Releases to Culebra in CRA-2019

In the CRA-2019, the fissile material reaching the Culebra, using the calculated flow rates and concentrations of fissile material, was generally low. The largest releases to the Culebra occur from the drilling intrusion scenario \mathcal{A}_{E1} and scenario \mathcal{A}_{E21} . In scenario \mathcal{A}_{E1} , a human exploring for minerals drills through the repository and into a hypothetical underlying brine pocket. Later, the driller plugs the borehole using concrete (present-day technology) and abandons it. Releases over the long term occur from hypothetical degradation of the concrete seal 200 years later and migration of radioisotopes to the Culebra brine saturated zone above the repository (Fig. 9).^o

In scenario \mathcal{A}_{E21} , an inadvertent intrusion into the repository occurs sometime after closure; a second intrusion borehole into repository and Castile brine pocket occurs later. The concrete plug in lower portion of second borehole fails 200 years later forcing flow through entire repository and up the first intrusion borehole. In both scenarios, salt creep isolates the Castile brine pocket 1200 years after the initial intrusion (Table VIII).

The 3 intrusion scenarios were further divided into computational scenarios (CS) based on the time of intrusion (Table VIII). The largest releases occur from intruding into the repository 100 years after closure. Computational scenario S6-BF-t100 has the potential to release the most Pu, but S6-BF does not involve a transport calculation from the repository to the Culebra. Rather, the mixing Pu concentration/mass in the repository is just placed in the Culebra in the analysis. Although these large S6-BF releases are considered in the release CCDF, they are not appropriate for making comparisons for criticality. Rather, the analysis uses the largest release that does involve a transport calculation from the repository up the borehole, computational scenario S2-BF-t100 (Table VIII).

In the WIPP PA, the repository exposure pathway model calculates a range of future repository behavior. The components are the (1) salt creep closure of the disposal rooms (SANTOS),⁶⁰ expressed as a porosity surface; (2) brine seepage into a disposal room and gas generation of H₂ from anoxic metal corrosion and CO₂, CH₄, and H₂S from

^m The calculation assumes drinking 2 L/d of water is the sole source of exposure: $0.15 \text{ mSv/y} \bullet 2 \text{ L/d} \bullet f^{ingest} \bullet 2.7 \times 10^{-3} \text{ d/y}$ where f^{ingest} is the ingestion dose factor⁵⁹ and equal to $1.4 \times 10^7 \text{ Bq/Sv}$ for ^{235}U and 10^6 Bq/Sv for ^{239}Pu and conversion factor is $2.7 \times 10^{-11} \text{ Ci/Bq}$.

ⁿ The calculation is as follows: $5.6 \text{ pCi/L} / (w_{239\text{Pu}} \bullet m_{239\text{Pu}})$ where $w_{239\text{Pu}}$ is the activity conversion factor of $6.2 \times 10^{-2} \text{ Ci/g}$ and $m_{239\text{Pu}}$ is the molecular weight of ^{239}Pu .

^o Solid, continuous concrete plugs are expected to remain intact for the 10,000-year regulatory period. Only segmented plugs are assumed to degrade. Hence, a probability of failure is associated with the type of plugs used to seal the abandoned borehole.

organic material degradation (BRAGFLO);⁶¹ and (3) dissolution of radionuclides into the brine (EQ3/6),³⁷ and then transport of radionuclides within the repository and up an intrusion borehole (NUTS)³³ (Fig. 10). Three replications of the calculations, each with a different starting random number, were run to evaluate potential variation in results. In each replicate, only a few simulations of the S2-BF-t100 computational scenarios show extensive Pu releases and occur when the uncertainty of Pu^{III} is near a factor of 933 (Table IV). In the first replicate (r1), Run 7 (out of 100) had the largest cumulative Pu release (610 kg). In r2, Run 68 had the largest Pu release (850 kg). In r3, Run 66 had the largest Pu release (92 kg) (Table IX and Fig. 11).

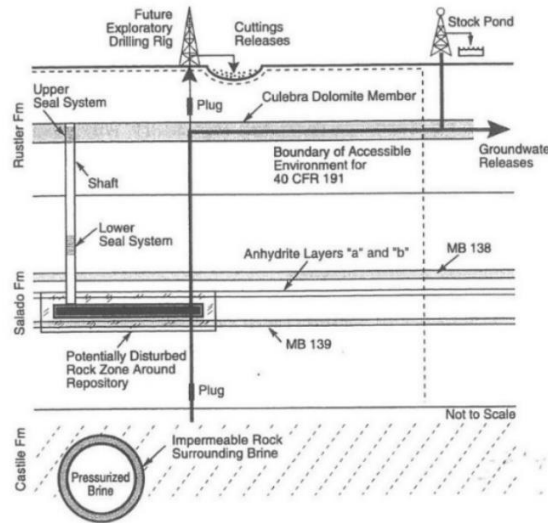


Fig. 9. Hypothetical future of release of radionuclides to the Culebra Member of Rustler Formation after disruptive human intrusion event into repository^{1, Fig. 2; 23, Figure 5.1-2}

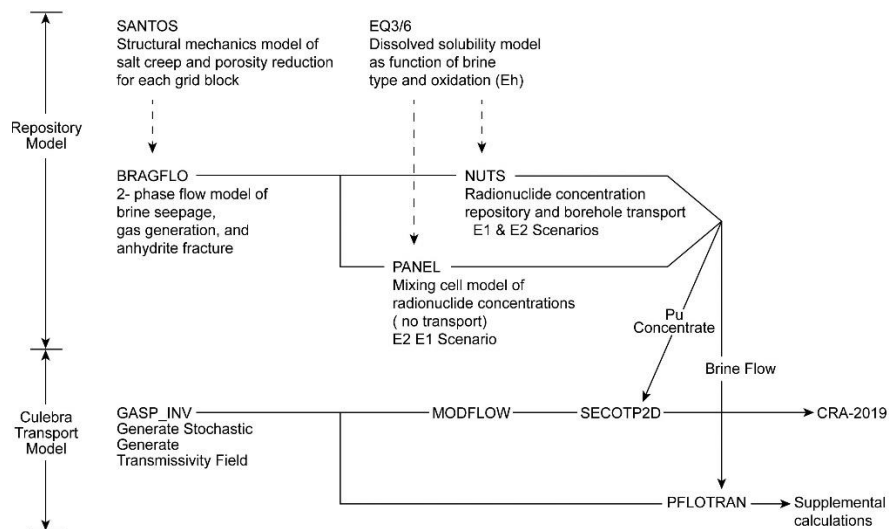


Fig. 10. Computational codes in the repository exposure pathway model that evaluate hypothetical futures of releases into the Culebra for Scenarios E1, E2, and E2E1^{13, Fig. 15}

Table VIII. Designation of Computational Scenarios for Modeling Intrusion into the WIPP Repository

ID	Short Description	Description
S1-BF	Undisturbed or Base Case (\mathcal{A}_U)	Predicted behavior of the WIPP disposal system when not disrupted by human intrusion or unlikely natural events
S2-BF-t100 S2-BF-t350	E1 intrusion after 100 and 350 years (computational components of scenario class \mathcal{A}_{E1})	Inadvertent intrusion into the repository and pressurized brine reservoir in the Castile 100 (or 350) years after closure; flow up to Culebra occurs 200 years later when borehole concrete plug fails; salt creep isolates Castile brine pocket 1200 years after intrusion; radionuclide transport in repository and up intrusion borehole based on brine flow calculation with intrusion at 350 years but with intrusion time shifted to 100 years for 100-year simulation.
S3-BF-t1000 S3-BF-t2000 S3-BF-t4000 S3-BF-t6000 S3-BF-t9000	E1 intrusion after 1000, 2000, 4000, 6000, and 9000 years (components of \mathcal{A}_{E1})	Inadvertent intrusion into the repository and pressurized brine reservoir in the Castile 1000 (or 2000, 4000, 6000, 9000) years after closure; flow up borehole to Culebra occurs 200 years later when plug fails; salt creep isolates Castile brine pocket 1200 years after initial intrusion; radionuclide transport in repository and up intrusion borehole based on brine flow calculation with intrusion at 1000 years but with intrusion time shifted to 2000, 4000, 6000, and 9000 years.
S4-BF-t100 S4-BF-t350	E2 intrusion after 100 and 350 years (components of \mathcal{A}_{E2})	Inadvertent intrusion into the repository 100 (or 350) years after closure; radionuclide transport up intrusion borehole occurs 200 years later when concrete plug fails
S5-BF-t1000 S5-BF-t3000 S5-BF-t5000 S5-BF-t7000 S5-BF-t9000	E2 intrusion after 1000, 3000, 5000, 7000, and 9000 years (components of \mathcal{A}_{E2})	Inadvertent intrusion into the repository 1000 (3000, 5000, 7000, 9000) years after closure; radionuclide transport up intrusion borehole occurs 200 years later when concrete plug fails
S6-BF-t100 S6-BF-t350 S6-BF-t1000 S6-BF-t2000 S6-BF-t4000 S6-BF-t6000 S6-BF-t9000	E2 then E1 intrusion after 100, 350, 1000, 2000, 4000, 6000, 9000 years (components of \mathcal{A}_{E2E1})	Inadvertent intrusion into the repository sometime after closure; 2 nd intrusion borehole into repository and Castile brine pocket later at 100 (or 350, 1000, 2000, 4000, 6000, 9000) years after closure; plug in lower portion of 2 nd borehole fails 200 years later forcing flow through entire repository and up 1 st intrusion borehole; lower portion of 2 nd borehole creeps shut 1200 years after 2 nd intrusion; radionuclide transport in repository and up intrusion borehole based on brine flow calculation with 2 nd intrusion at 2000 years but with 2 nd intrusion time shifted to 100, 350, 1000, 4000, 6000, and 9000 years.

Table IX. Mean and maximum cumulative brine and Pu releases to Culebra in S2-BF-t100 of CRA-2019

Scenario	Replicate	Brine			Pu			
		Mean (m ³)	Max (m ³)	Max Run	Mean (kg)	Max (kg)	Max Brine (m ³)	Max Run
S2-BF-t100	r1		152 000	17	9.01	609.74	95 300	7
	r2		75 900	36	14.19	853.23	72 000	68
	r3		129 000	66	1.38	91.93	129 000	66
	Average				8.19			
S2-BF ^a	Average	4 720	7 540					

^aSee Table VII

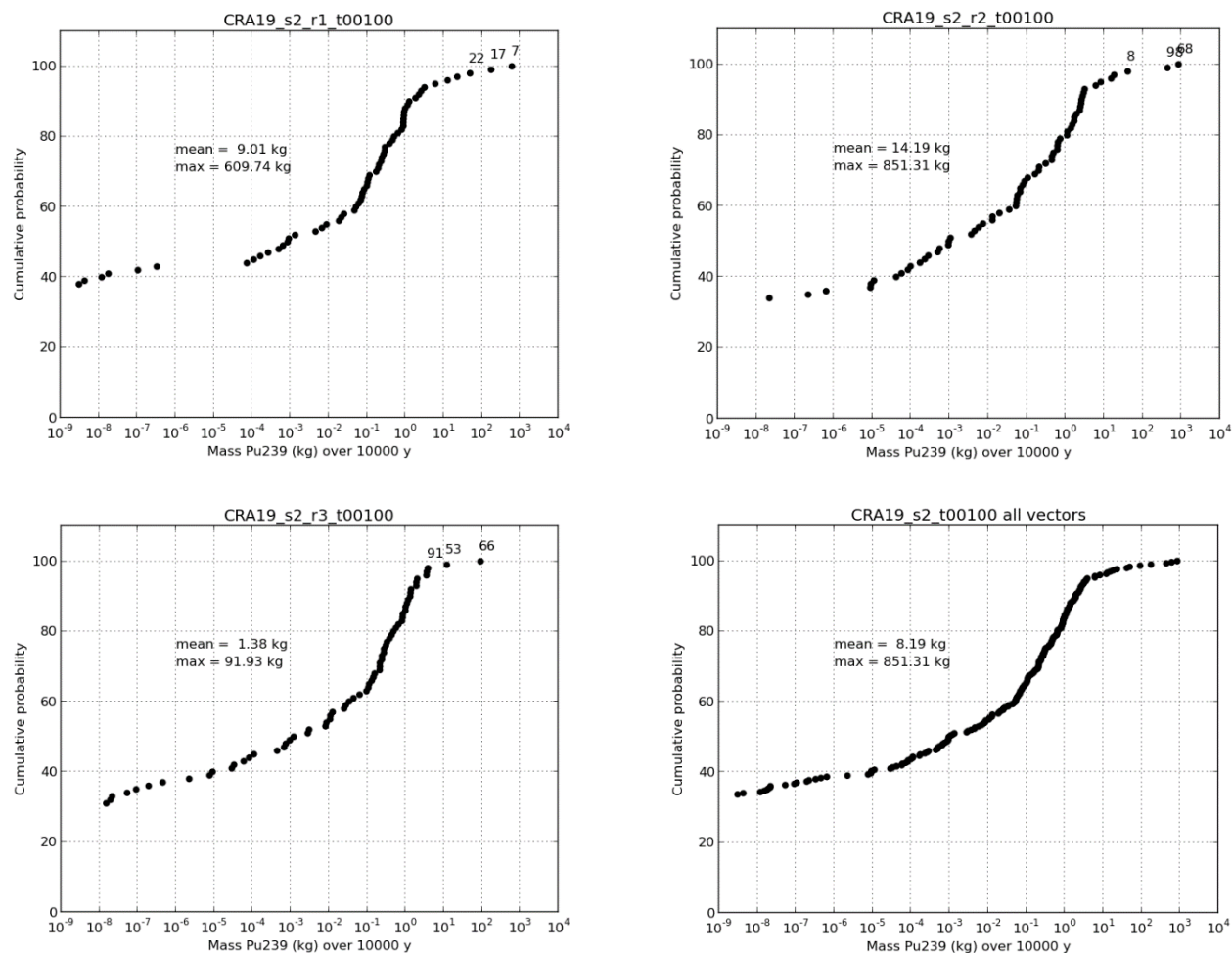


Fig. 11. Distribution of Pu releases to Culebra in each of 3 replicates and in all replicates combined for computational scenario S2-BF-t100 in CRA-2019.

The ²³⁹Pu releases are approximately lognormally distributed. Hence the largest releases are several orders of magnitude greater than the means. As an example, we have calculated the mean for all three replicates of S2-BF-t100 of CRA-2019 (Fig. 11). The mean release of 8.2 kg Pu conditional on S2-BF-t100 occurring is a factor of 104 less than the maximum of 851 kg.^p This mean of 8.2 kg of Pu is a factor of 1.75 larger than the mean of 4.7 kg Pu in the CCA-1996 (from S5-BF-t1000). This factor of 1.75 increase is not as dramatic as the factor of 8 increase when comparing worse case releases (i.e., 110 kg in the CCA-1996 versus 851 kg in S6-BF-t100-r1 of CRA-2019). The large uncertainty associated with Pu^{III} solubility noted in Table IV contributes to this difference.

The maximum Pu releases are associated with high brine releases, but not necessarily the largest (Table IX, Fig. 12, Fig. 13, and Fig. 14).

^p The mean Pu release for the entire PA is larger because multiple intrusions of S1-BF through S6-BF may occur, however, we use the Pu release in each of the individual intrusions because each intrusion occurs in a separate location and two intrusions are not likely to occur close enough to combine masses in a small radius.

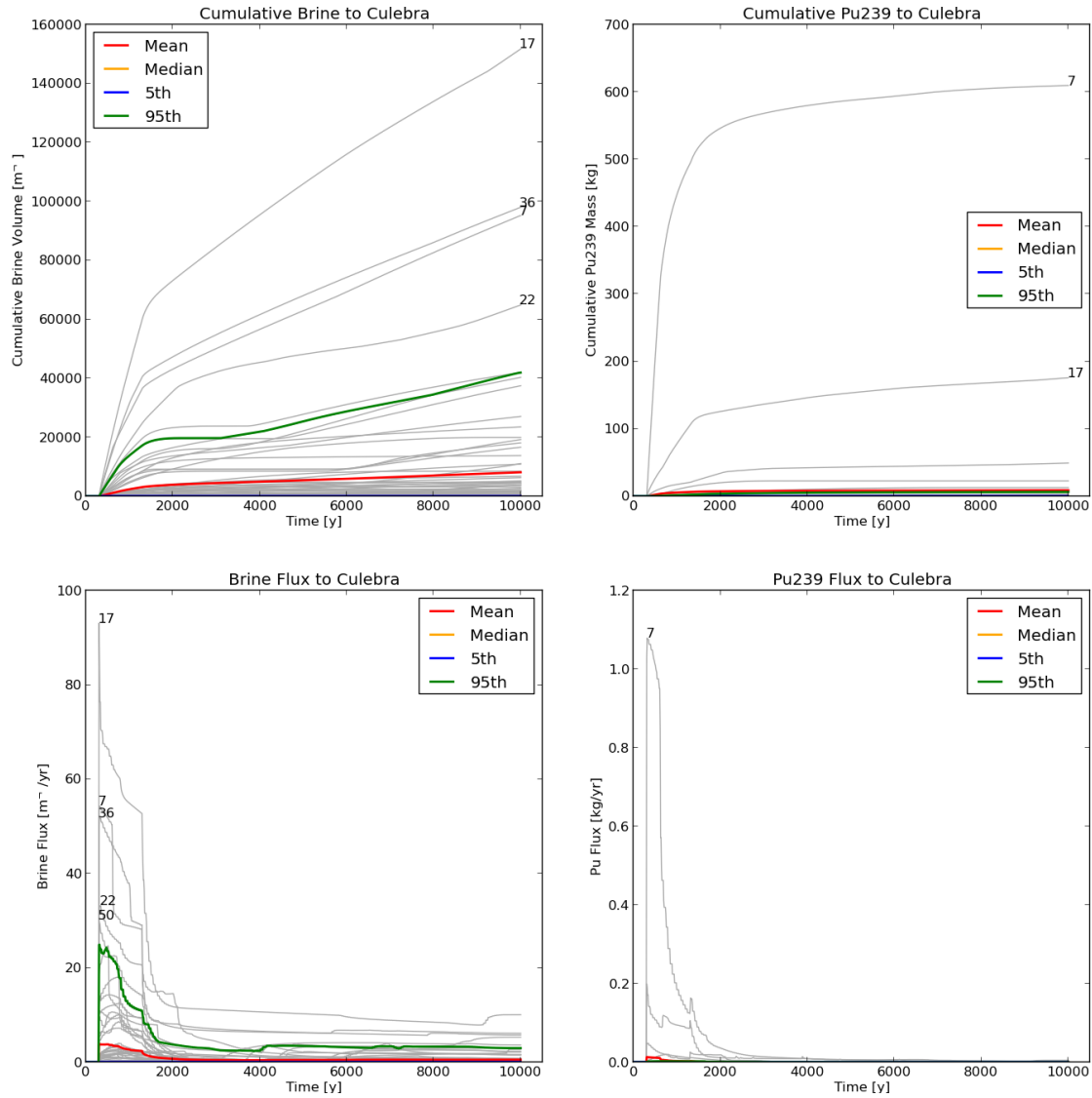


Fig. 12. Cumulative volume and flow rate of brine and cumulative Pu mass and flux into Culebra over 10,000 years from an intrusion that occurs 100 years after closure in replicate 1 of CRA-2019 (S2-BF-t100-r1).

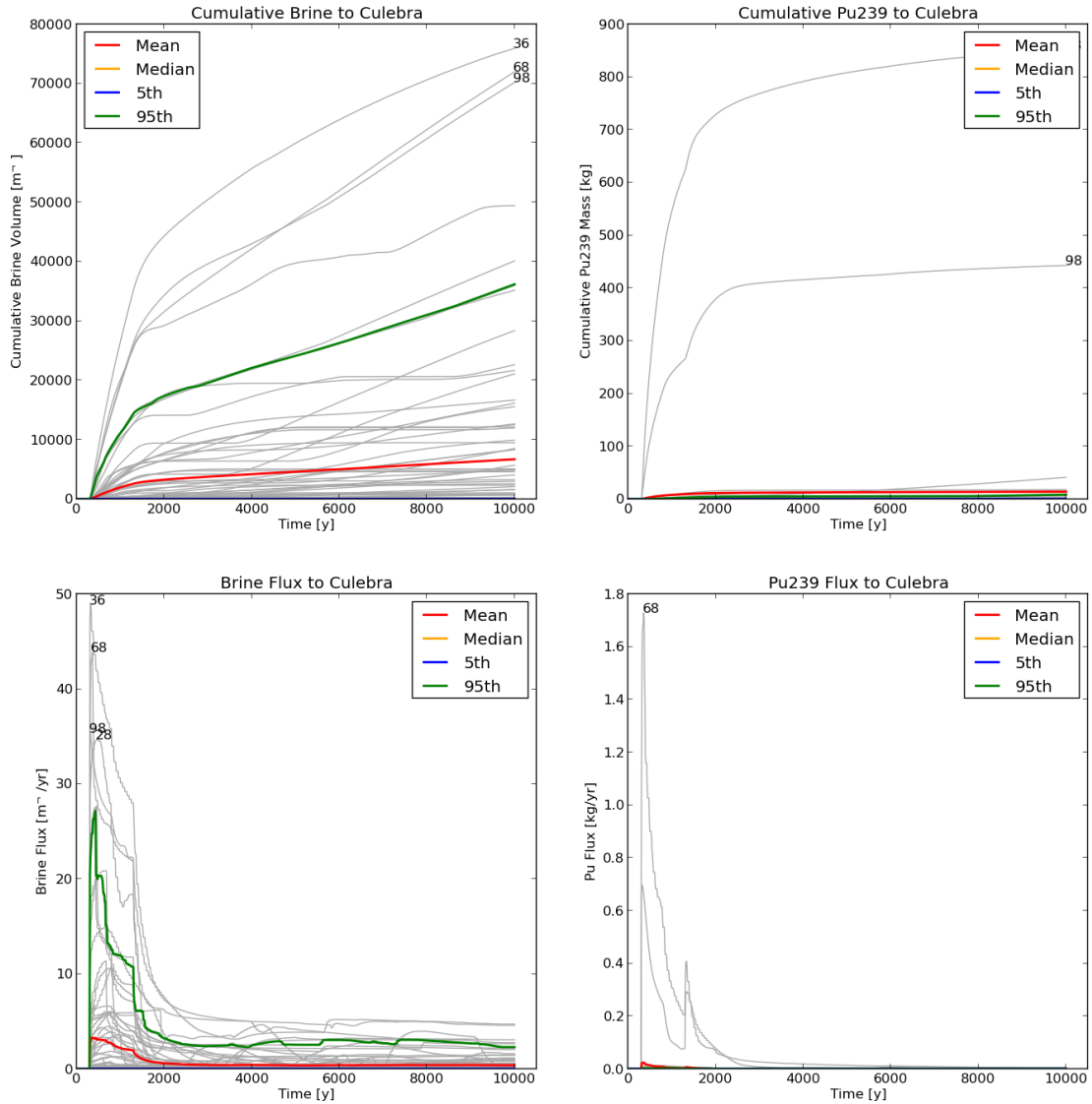


Fig. 13. Cumulative volume and flow rate of brine and cumulative Pu mass and flux into Culebra over 10,000 years from an intrusion that occurs 100 years after closure in replicate 2 of CRA-2019 (S2-BF-t100-r2).

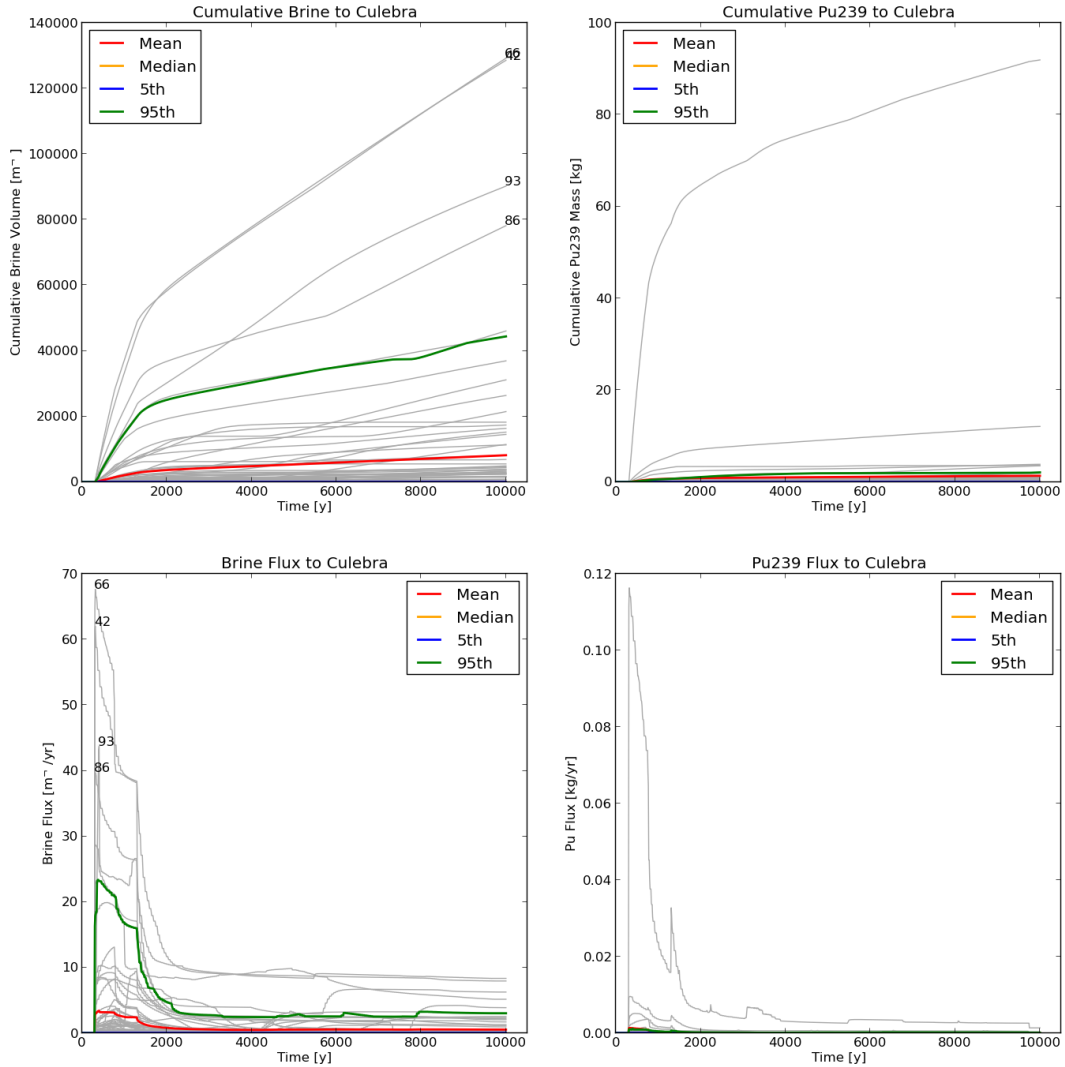


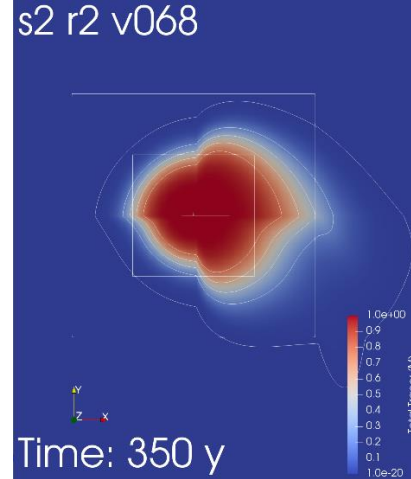
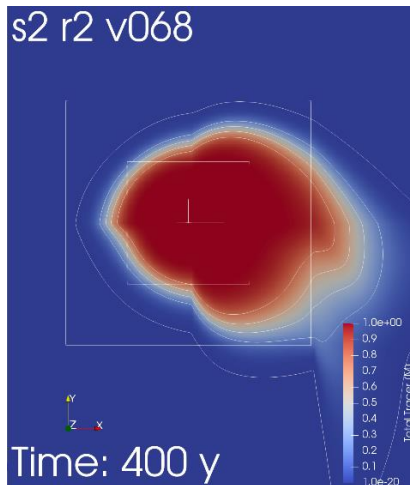
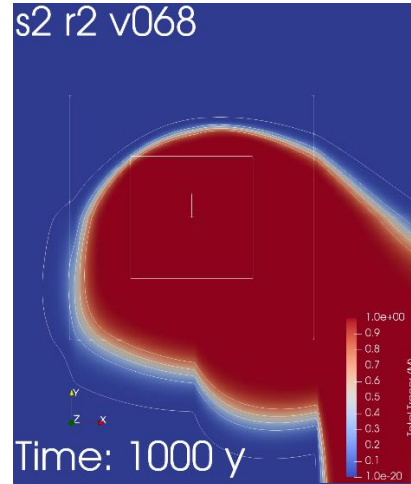
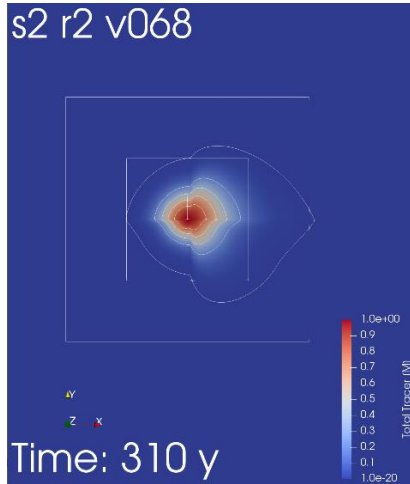
Fig. 14. Cumulative volume and flow rate of brine and cumulative Pu mass and flux into Culebra over 10,000 years from an intrusion that occurs 100 years after closure in replicate 3 of CRA-2019 (S2-BF-t100-r3)

VII.B.2 Supplemental Analysis of Pu Dispersion in Culebra

Generally, the CRA-2019 performance assessment evaluates radionuclide transport in the Culebra dolomite on a macroscale using MODFLOW and SECOTP (Fig. 10). While not yet fully qualified for use in PA calculations demonstrating compliance, supplemental simulations were made on a microscale with PFLOTRAN version 1.01,⁶² to provide additional justification to conclusions based on qualitative arguments. Specifically, supplemental simulations evaluated the size of the zone in which dilution and potential precipitation might occur because of changes in ionic strength or pH. The boundary conditions were the same as for regional flow model in CRA-2019, and the regional flow fields from PFLOTRAN are identical to CRA-2019.⁴ Because of the corresponding large solubility and thereby

⁴ PFLOTRAN will replace MODFLOW and SECOTP in the future. However for CRA-2019, the PFLOTRAN capabilities used here were qualified for this application.⁶³ The input and output files are located in the WIPP central files as /nfs/data/CVSLIB/WIPP_EXTERNAL/CRA19_crit/FILES.

Pu releases, one supplementary simulation used information from Run 68 of S2-BF-t100-r2. The maximum cumulative brine flow to the Culebra is 72 000 m³ over 10⁴ years (Table IX). This large brine flux causes a major perturbation in the Culebra flow field. The second supplementary simulation used the mean brine flux from all 100 runs of S2-BF-t100-2r (7000 m³ cumulative brine value, which is more than an order of magnitude less) to evaluate a situation with much less perturbation of the Culebra flow field.



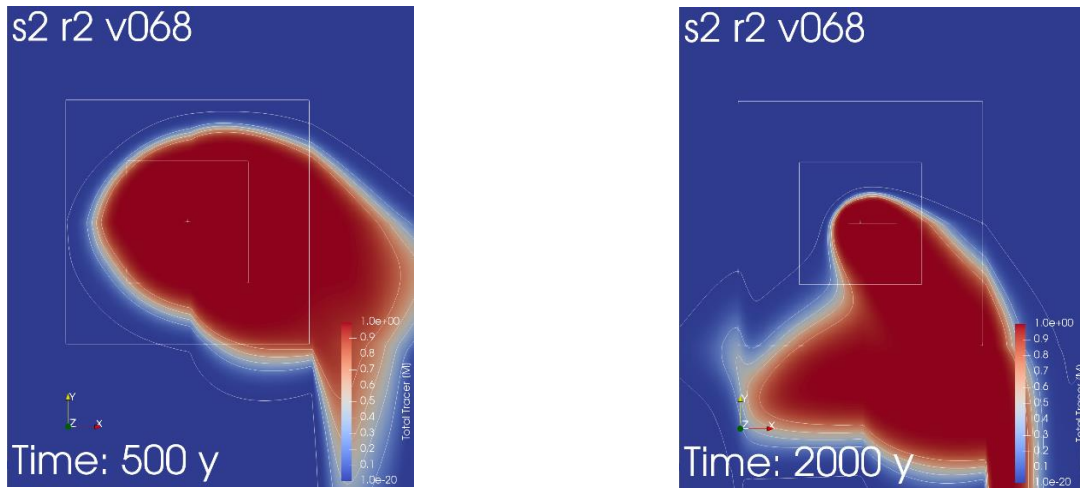
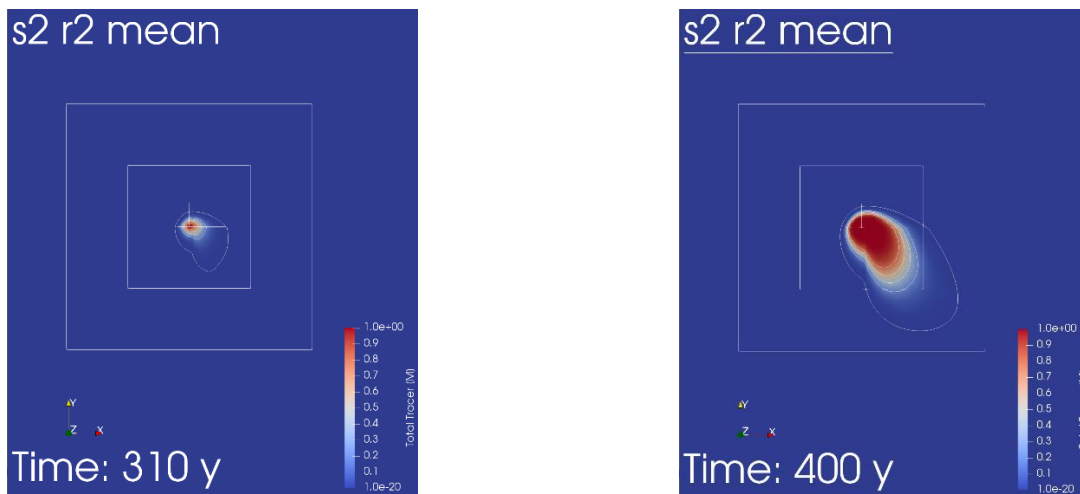


Fig. 15. Plume of non-adsorbing tracer in Culebra at intrusion borehole between 310 years and 2000 years with brine flux of 72 000 m³ in run 68 of computational scenario S2-BF-t100-r2; lines at borehole are 5 m, 10 m, and 15 m long; boxes are 50 m and 100 m on a side; contours are at normalized tracer release of 0.001, 0.2, 0.4, 0.6, and 0.8.



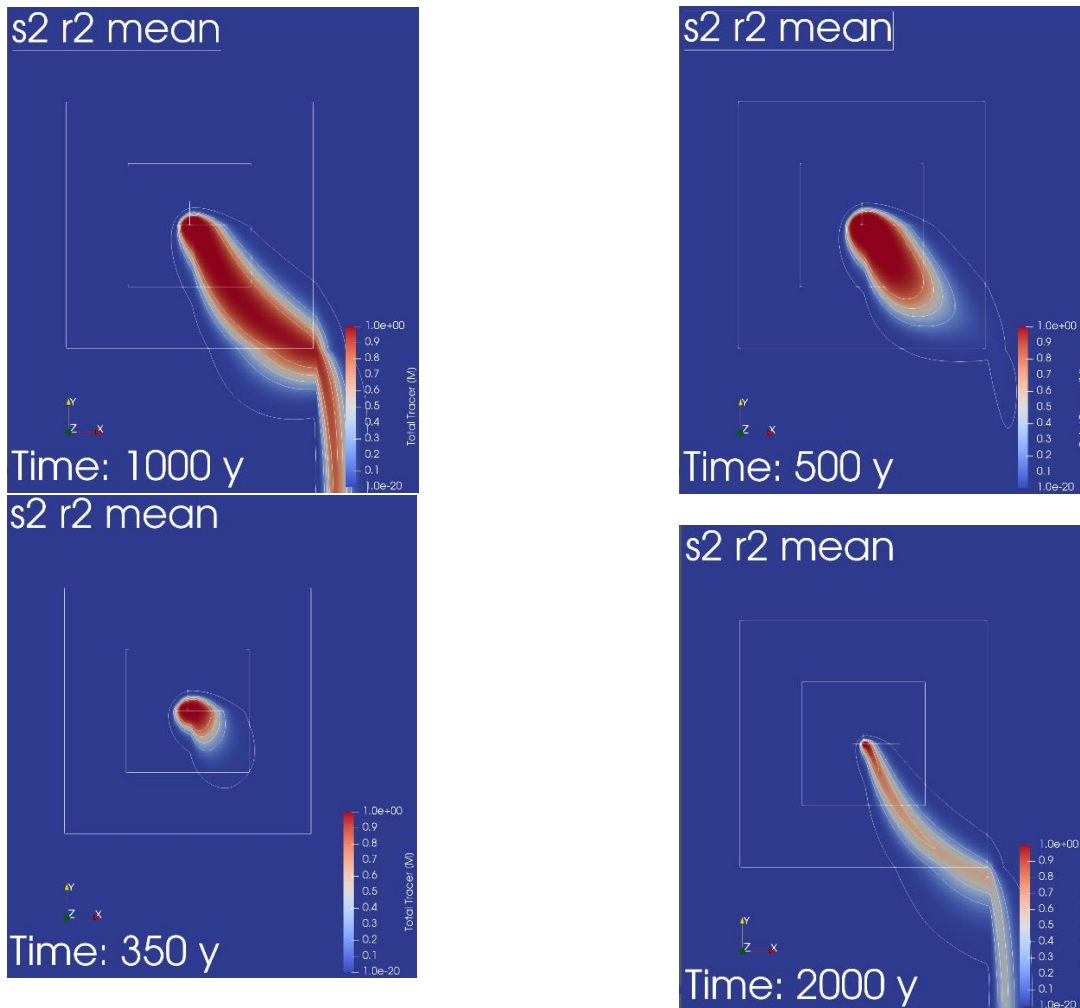


Fig. 16. Plume of non-adsorbing tracer in Culebra at intrusion borehole between 310 years (10 years after plug to Castile brine pocket fails in 100-year intrusion) and 2000 years (800 years after salt creep closes off Castile brine pocket) with mean brine flux of all 100 runs of scenario S2-BF-t100-r2.

In WIPP PAs, the uncertainty in fluid flow is represented by 100 Culebra flow fields generated from 100 conditioned transmissivity fields (GRASP_INV in Fig. 10). In these 100 flow fields, the uncertainty in fluid flow directly above the disposal waste panels, as represented by the standard deviation of the Darcy velocity, is small (Fig. 17). The Darcy velocity variability is small because several wells measurements above the near the repository constrain the variability. The microscale of our calculations is about 100 m and thus within the 629-m by 776-m boundary of the disposal panels (Fig. 18). Consequently, it does not matter which flow field is chosen for our calculations. We chose the first flow field generated.

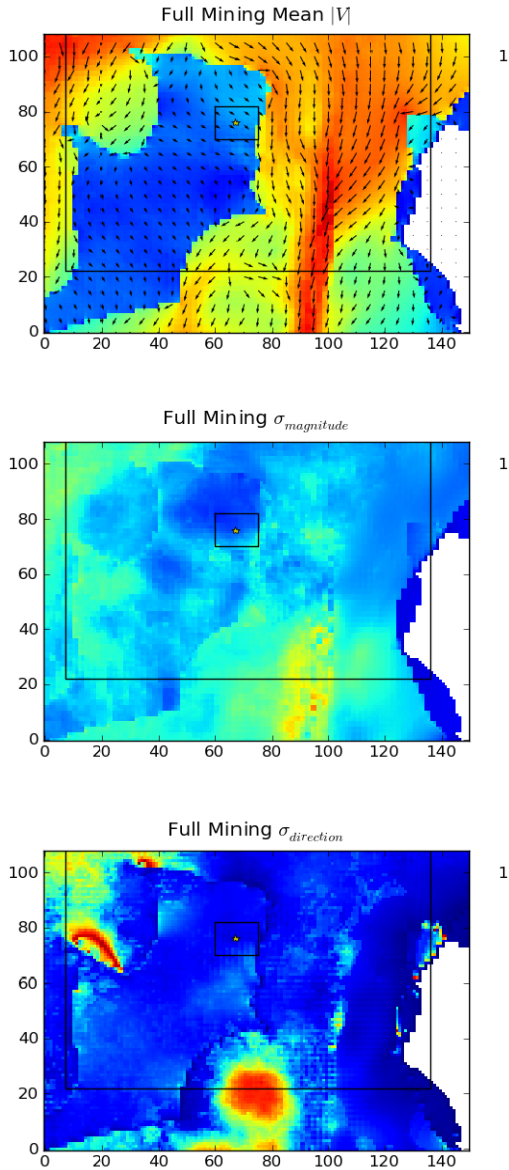


Fig. 17. Average Darcy velocity magnitude (between 10.5 and 9.0 m/s above WIPP panels), standard deviation magnitude (between 0 and 0.6 m/s above WIPP panels), and directional standard deviation (between 0 and 0.3 of $\tan^{-1}(v_y/v_x)$ above WIPP panels) of 300 flow fields (3 replicates of 100) for the scenario where potash mining disrupts the Culebra flow field. The small black box is the outline of the WIPP panels; the larger black box is the land withdrawal boundary.^{64, Figure 4-3}

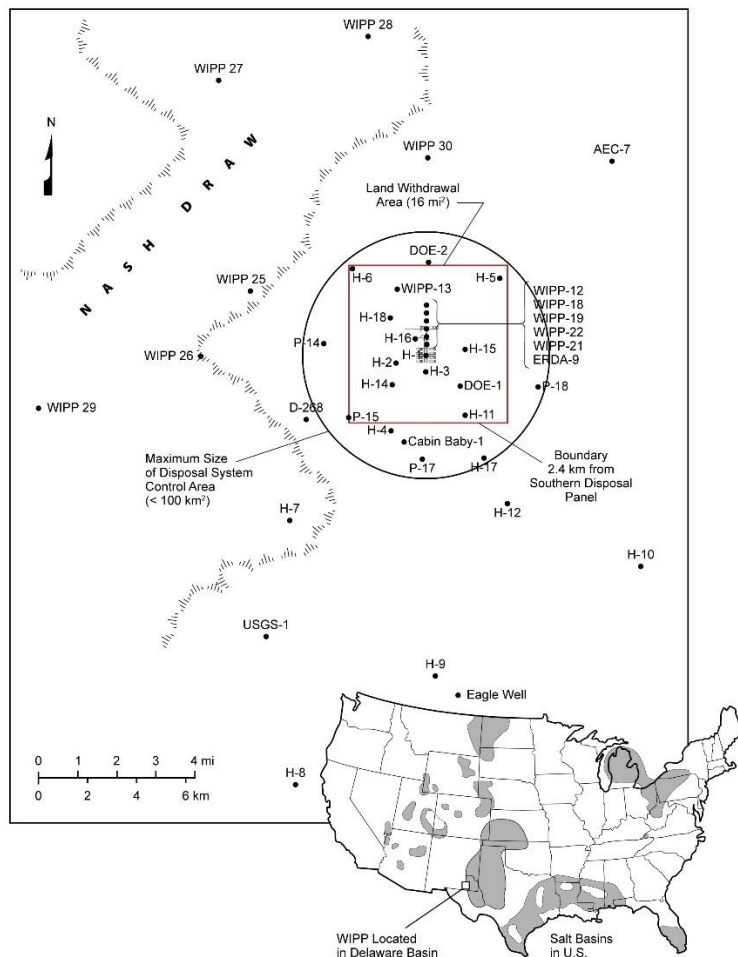


Fig. 18. Wells near the WIPP land withdrawal boundary and WIPP disposal panels

VII.C. Geochemical Constraints on Concentration Mechanisms in Culebra

VII.C.1. Conditions for Precipitation in Culebra

Change in Ionic Strength. As WIPP repository brine enters and mixes with Culebra brine, the ionic strength will drop from between 6700 and 5300 mM to 800 mM (Table II). Solubility of most highly negatively charged species are stabilized by high ionic strength so that a mineral whose solubility is controlled by highly charged species in solution will have a higher solubility in high ionic strength brines. Hence, as the brine is diluted, the solubility could decrease. Consequently, a possible situation is the dilution of Pu^{III} in a Castile-dominated brine to a Culebra-dominated brine.

Change in pH. The pH and CO_2 concentration in the repository is controlled by the addition of excess MgO to form brucite, $\text{Mg}(\text{OH})_2$, at a buffered pH of 9. Contaminated brines entering the Culebra will carry dissolved $\text{Mg}(\text{OH})_2$, but little solid MgO , so the pH could drop from alkaline to near neutral of the Culebra brine (Table II), and the CO_2 concentration rise, as the $\text{Mg}(\text{OH})_2$ was consumed by the Culebra CO_2 to form hydromagnesite $\text{Mg}_5(\text{CO}_3)_4(\text{OH})_2 \cdot \text{H}_2\text{O}$. The change in pH and CO_2 concentration could cause co-precipitation of plutonium or uranium with MgCO_3 within the Culebra pore space; however, changes in pH and availability of CO_2 would still be dependent on sufficient mixing of the two brines.

Modeling brine mixing. The large perturbation of the Culebra flow field by the injection of $\sim 72\,000\text{ m}^3$ of Castile brine at the intrusion borehole results in an initially large mixing zone for the largest release (run 68 of S2-BF-t100-r2). Based on the normalized concentration contours between 0.2 and 0.8 of a non-adsorbing tracer, the mixing zone is $\sim 1180\text{ m}^2$ in the first 10 years assuming a circular annulus with a minimum radius of 5 m and maximum of 20 m (Fig. 15).

Although the annulus width of the mixing zone decreases at later times, the diameter keeps increasing such that the mixing zone area increases by a factor of 1.5 (1810 m^2 with 8 m annulus at 32 m radius—Table X). If one uses the Pu flux rate of run 68 of S2-BF-t100-r2 (Fig. 13), a rough estimate of the concentration in the mixing zone is possible. Although the 294 kg Pu mass released between 500 and 1000 years of CRA-2019 is large, the volume is so large (even when assuming deposition in only one meter of the 4-m thick Culebra) that the Pu concentration of 0.25 kg/m^3 (Table X) remains a factor of 15 below the critical concentration of 3.7 kg/m^3 in Table VI (i.e., the mixing volume must be a factor of 15 smaller at a 1000 years).

Table X. Mixing zone and corresponding Pu solid concentration for intrusion at 100 years and Castile plug failure 200 years later in CRA-2019 (S2-BF-t100-r2)

Time since WIPP Closure (y)	Time since Castile Plug Failed (y)	Cumulative Pu Released in CRA-2019 (kg)	Pu Flux	Mixing Radius to 0.8 contour (m)	Annulus to 0.2 contour (m)	Volume ^a (m ²)	Pu Conc (kg/m ³)
Area of mixing of $\sim 72\,000\text{ m}^3$ brine flow (cumulative) of S2-BF-t100-r2 for run 68 (Fig. 15)							
310	10	11		5	15	1180	0.001
350	50	76	65 ^b	23	9	1560	0.04
400 ^c	100	151	75	32	8	1810	0.04
500	200	256	105	35	7	1690	0.06
1000	700	550	294	35	5	1180	0.25
Mixing area for mean brine flow (7000 m^3 total) and 8.2-kg mean Pu release in S2-BF-t100-r2 (Fig. 16)							
310	10	2.23		1	3	47	0.047
350 ^d	50	8.2 ^e		5	3	123	0.067

^aVolume assumes 1 m flow thickness in 4-m thick transmissive Culebra dolomite

^bBecause the mixing zone changes location, only the difference between successive time steps is used (e.g., 310 and 350 years); however, even assuming the entire mass released was in the mixing zone would not cause criticality.

^cThe mixing area remains fairly circular through 400 years because of the large brine flux from the borehole

^dThe mixing area transitions to a more traditional elliptical shape after 350 years

^e8.2 kg is cumulated over 10 000 years (Fig. 11)

The mean brine flux rate perturbs the Culebra regional flow field much less, and the zone of mixing is between 47 m^2 and 123 m^2 in the first 10 and 50 years, respectively (Fig. 16). However, the Pu concentration of remains orders of magnitude below the critical concentration of 3.7 kg/m^3 (Table X).

Although an exhaustive search of the probabilistic combinations to find a situation of a minimum flow field disturbance and maximum Pu discharge could be conducted, the order of magnitude variation in brine flow simulated here spans the range of behavior. Over this range of behavior, the Pu concentration remains orders of magnitude below the critical concentration of 3.7 kg/m^3 . Consequently, the simulations suggest chemistry changes from mixing will likely occur over a wide area as the injected brine flux varies with time.

VII.C.3. Geochemical Constraint on Adsorption in Culebra

While precipitation would occur in the mixing zone between the Salado/Castile brine and Culebra brine as the brine chemistry changed, adsorption would tend to occur next to the borehole. These two zones do not overlap except during the initial Pu release. By 10 years, the zones have diverged. For the Pu^{III} discharge of 188 kg at 10 years in S2-BF-t100-r1 of CRA-2019 (Table X), the maximum cylinder radius is 2.2 m to reach a critical concentration of 12 kg/m³ in Salado or Castile brine, which would be the dominate fluid at the borehole (or 4.5 m to reach a critical concentration of 3.7 kg/m³ in Culebra brine—Table VI) assuming deposition in one meter of the 4-m thick Culebra. In comparison, the radial distance to the mixing zone is already 5 m at 10 years when the cumulative brine discharge is 72,500 m³. Similarly for the mean Pu^{III} release of 2.23 kg at 10 years, the maximum cylinder radius is 0.24 m in Salado Castile brine (or 0.5 m in Culebra brine). In comparison, the radial distance to the mixing zone at 10 years is 5 m when the cumulative brine discharge is 7000 m³ (Table X).

VII.C.4. Geochemical Constraint on Colloidal Filtration in Culebra

Because the total mobile concentration of Pu^{IV} is due partially to microbial and mineral colloids, filtering or destabilizing these colloids could lead to a possible means of Pu deposition in the Culebra. Colloidal destabilization occurs primarily because of changes in ionic strength which at WIPP occurs over a large brine mixing zone too large to cause criticality (as already discussed for precipitation).

Colloids susceptible to filtering would likely be filtered during transit through waste within the repository or in the borehole backfill material; however, to be consistent with the assumptions for the PA, colloids were assumed to have escaped the repository and borehole and then be filtered or destabilized in the Culebra. For simulations with Pu solubility at its extreme uncertainty, the filterable colloid fraction is miniscule (Table VIII).

To exceed critical concentration at mean values of Pu concentration, colloids must filter at the borehole (like adsorption); yet, the filterable fraction barely approaches the minimum critical mass and the critical concentration associated with the minimum critical mass cannot be reached. To elaborate, the largest filterable fraction is associated with Pu^{IV} for simulations with solubility near the mean. In either Salado or Castile brine, Pu^{IV} associated with filterable mineral and microbial colloids accounts for 28% of the Pu total concentration (Table VIII). Perfect filtering of 28% of the mean 14 kg Pu released in S2-BF-t100-r2 (Table IX) results in 3.9 kg, which is less the 9.7-kg critical mass in Salado brine and the 7.5-kg critical mass in Castile brine.

More importantly, filterable mineral and microbial colloids adsorb Pu externally (e.g., on the cell surface); thus, this adsorption is controlled through equilibrium with the solution concentration. The link between colloidal concentration and equilibrium thermodynamics creates a limit on the concentration of colloidal fissile material that cannot reasonably exceed by many orders of magnitude the dissolved concentration of Pu and, thereby, go critical. Pu adsorbed on colloids would readily de-adsorb from a collection of filtered colloids.

VIII. SUMMARY

Hydrologic and geochemical processes cannot sufficiently concentrate fissile material (consisting primarily of ²³⁹Pu but also ²³⁵U) to cause criticality in and around the Waste Isolation Pilot Plant (WIPP), an operating repository in bedded salt for geologic disposal of TRU waste from atomic energy defense activities. Based on (1) the qualitative low-probability rationale, presented here; and (2) the rationale that salt creep compaction also cannot sufficiently

concentrate fissile material, presented in a companion memorandum, criticality events are not considered in the 2019 Compliance Recertification of WIPP. This situation is true even when considering the disposal of TRU waste in pipe overpack containers (POCs) and potential disposal of non-pit surplus plutonium with high initial concentrations of fissile ^{239}Pu in criticality control overpacks (CCOs).

Herein, the probability of criticality is notionally conceived as the sum of the low probability of fluid flow, dissolution, precipitation, sorption, and colloidal aggregation sufficiently concentrating fissile material in the repository and geologic barrier prior to and after disruption of the WIPP disposal system by inadvertent human intrusion. The improbability of criticality for these situations is as follows.

VIII.A. Hydrologic and Geochemical Constraints within Repository Prior to Hypothetical Human Distruption

After extensive container degradation but prior to inadvertent intrusion by exploratory drilling into WIPP, hydrologic conditions constrain the location, sufficiency of brine, and contribution to mixing. Specifically, brine from the host salt seeps into the repository rather than out, preventing deposition of fissile ^{239}Pu and ^{235}U in adjacent geologic strata. In some simulations, brine seepage is completely consumed by anoxic corrosion of steel containers, in which case, no gradient exists to move fissile material. For those hypothetical situations with large brine inflow, a small 1% dip of the Salado host bedded salt contribute to more uniform mixing of high concentrations of fissile material disposed in northern panels (such as POCs in Panels 1 and 2, and non-pit Pu possibly disposed in Panel 10— Fig. 4) with lower concentrations in southern panels of the repository (Table XI).

An important constraint on geochemical conditions within the WIPP repository is the fairly uniform distribution of iron in the containers and magnesium oxide (MgO) added in the repository, which keeps the brine chemistry fairly uniform such that pH, ionic strength, and reduction-oxidation potential do not vary widely. For example, MgO reacts with carbon dioxide produced from microbial degradation of organic material in TRU waste and keeps the pH uniformly mildly basic at ~9. In turn, the dissolved concentration of Pu^{III} or Pu^{IV} remains 3 to 5 orders of magnitude less than the critical limit in Castile brine (Table XI).

Other geochemical constraints prevent criticality prior to intrusion. The presence of reductants, adsorptive material, and colloid substrates, such as ubiquitous iron from waste containers, is well distributed throughout the repository on a macroscopic scale. Consequently, while precipitation, adsorption, or colloidal aggregation may occur on a microscopic scale, macroscopic conditions do not promote preferential deposition of sufficient quantities of Pu from between 15 and 200 drums at only one or a few locations (Table XI).

VIII.B. Hydrologic and Geochemical Constraints within Repository After Hypothetical Human Distruption

After human intrusion, brine flow may move fissile material within the repository. However, the addition of copious amounts of Castile brine from a hypothetical brine pocket below the WIPP does not substantially change pH, ionic strength, or the reduction-oxidation potential within the repository and promote sufficient precipitation, adsorption or colloidal aggregation to cause criticality.

VIII.C. Hydrologic and Geochemical Constraints in Culebra After Hypothetical Human Distruption

Hydrologic conditions constrain the deposition location of fissile material released through an intrusion borehole. The relatively greater permeability favors movement of fissile material to the Culebra dolomite above the repository

rather than to other strata. Furthermore, fluids tend to flow into rather than out of Culebra; thus, there is little likelihood of deposition in adjacent strata. The dispersion that normally occurs while contaminants move through the Culebra and the lack of known deposition zones suggests that the fissile material brought to the Culebra can only reach a critical concentration near the intrusion borehole. Yet, the typically low solubility of the fissile material implies that vast amounts of brine are required to transport a sufficient quantity of fissile material to cause criticality. The large amount and variability of the brine flux spreads out the mixing between the brine from the intrusion borehole and the brine in the Culebra. The subsequently large mixing zone is such that a concentration of 100% enriched ^{239}Pu greater than a criticality limit of 3.7 kg/m^3 (or a concentration of 5% enriched ^{235}U greater than a criticality limit of 160 kg/m^3) cannot be reached (Table XI).

Similar to the underground facility, several unfavorable geochemical conditions exist to prevent criticality within the Culebra. Uranium ore deposits in evaporates such as the Culebra dolomite are rare because carbonate in the formations increases rather than decreases solubility. Hence, a strong reducing agent is necessary to reduce U^{VI} to U^{IV} . Because a strong reductant (or oxidant) in a localized area has not been discovered within the Culebra, a sudden change in the reduction-oxidation potential is unlikely. More importantly, the 180 kg/m^3 critical concentration required for 5% enriched UO_2 in Culebra far exceeds concentrations found in economically mineable ores (14 kg/m^3 for 20% wt high-grade ore at 3000 ppm in dolomite).

The solubility of Pu^{IV} in PuO_2 increases with the carbonate abundantly available in the Culebra dolomite brine saturated zone. On the other hand, the solubility of Pu^{III} decreases in the Culebra dolomite brine (assuming organic complexing agents in the WIPP waste have combined mostly with the abundant Ca^{+2} available in the Salado, Castile, and Culebra brines). However, the large mixing zone within the Culebra mitigates any tendency to precipitate Pu^{III} in high concentrations. Precipitation would be gradual and diffuse over a large area. Any Pu deposition that occurred would have to at least exceed a low-grade ore concentration (i.e., 2.5 kg/m^3 for 1% wt low-grade ore at 1000 ppm) to reach a 3.7 kg/m^3 critical concentration.

Adsorption and colloidal destabilization/filtration are not likely mechanisms to form criticality concentrations of Pu. The entire adsorption capacity of dolomite is required to reach a critical concentration of 3.7 kg/m^3 for Pu; yet, adsorption is not exclusive to Pu. Other metal cations such as Ca^{+2} and Mg^{+2} in the Culebra brine readily exchange with Ca^{+2} and Mg^{+2} in the dolomite; hence, Pu must compete with brine components to dislodge already adsorbed metal cations. Furthermore, adsorption and precipitation would not necessarily work in tandem since adsorption would more likely occur at the borehole while precipitation would be at the mixing front.

Colloidal destabilization occurs primarily because of changes in ionic strength which occur over large brine mixing zone too large to cause criticality (like precipitation). To exceed critical concentration at mean values of Pu concentration, colloids must filter at borehole (like adsorption); yet the filterable fraction barely approaches the minimum critical mass and the critical concentration associated with the minimum critical mass cannot be reached. More importantly, filterable mineral and microbial colloids adsorb Pu externally; thus, adsorption is controlled in equilibrium with the solution concentration, which in turn, limits the ability of a collection of filtered colloids to exceed the solution concentration by many orders of magnitude (Table XI). For simulations with Pu concentration at its maximum from extreme uncertainty, the filterable colloid fraction is practically zero. For simulations with Pu

dissolved concentration at its mean, the dissolved concentration of Pu in Castile brine is 1.5×10^{-3} mM or 3.6×10^{-4} kg/m³ and the colloid concentration is only 28% of the total Pu concentration.

In several situations in this rationale, bounding results from the CRA-2019 were used for arguing that a qualitative estimate of the probability of criticality is very small and so the rationale for eliminating a criticality event will likely remain valid in future WIPP PAs. However, changes that would necessitate a re-evaluation include (1) use of extremely high solubility values for Pu^{III}, (2) non-uniform changes in the distribution of iron and MgO throughout the repository and (3) the discovery of geochemical conditions in the Culebra dolomite strata above the repository that would promote fissile material deposition other than simple mixing of repository brines with Culebra brines.

Table XI. Rationale for Low Probability of Criticality from hydrologic and geochemistry processes in WIPP Disposal System

Scenario Location Process	Rationale for Hydrologic/Geochemistry Not Causing Criticality
Undisturbed Repository Fluid Flow	Hydrologic Constraint on Depositional Location in Repository for Undisturbed Condition 1. Without intrusion, short-term gradient causes brine seepage <i>into</i> disposal rooms. 2. In some simulations, brine seepage is completely consumed by anoxic corrosion of steel containers, in which case, no gradient to move fissile material 3. For case with much brine seepage, 1% dip of strata contributes to more uniform mixing of fissile plutonium (²³⁹ Pu) at high fissile concentrations disposed in northern panels with waste in southern panels.
Dissolution	Geochemical Constraint on Dissolved Concentration in Salado Brine Maximum Pu ^{III} dissolved concentration of 0.17 mM or 0.04 kg/m ³ in Castile brine is 3 orders of magnitude <40 kg/m ³ criticality limit; maximum Pu ^{IV} concentration of 0.0015 mM or 3.5×10 ⁻⁴ kg/m ³ in Castile or Salado brine is 5 orders of magnitude <40 kg/m ³ criticality limit in Castile brine. Also, the ²³⁵ U concentration of 1 mM (0.235 kg/m ³) is 4 orders of magnitude <2800 kg/m ³ criticality limit in Salado brine.
Precipitation	Geochemical Constraint on Precipitation Concentration Reducing agent, such as iron (Fe ⁰) from drums, and added MgO carbonate reactant well distributed, on macroscopic scale, throughout waste and repository, which keeps brine chemistry fairly uniform and thereby no preference for precipitation. Specifically, magnesium oxide (MgO) reacts with carbon dioxide (CO ₂) and thereby keeps pH uniformly basic at ~9. Furthermore; reduction of non-pit Pu ^{IV} as PuO ₂ to Pu ^{III} increases Pu solubility
Adsorption	Geochemical Constraint on Adsorption Concentration 1. Adsorptive material such as rust well distributed throughout waste and repository 2. Adsorption not exclusive to fissile material; readily available metal cations in the seeping brine such as Ca ⁺² and Mg ⁺² compete for adsorptive sites 3. Adsorption of Pu ^{IV} does not exceed critical concentration for mixture with rust of 26 kg/m ³ in Salado brine
Colloid Agglomeration	Geochemical Constraint on Colloid Agglomeration Concentration 1. Substrates for colloid formation well distributed throughout repository; gravitational settling following destabilization of mobile colloids does not cause large colloid agglomerations (like dust settling in a closed room) 2. No bioaccumulation occurs by microbes; rather Pu adsorbed on cell wall.
Intrusion Repository Precipitation	Geochemical Constraint on Precipitation Concentration in Repository after Intrusion 1. Fe ⁰ reducing agent from drums and added MgO carbonate reactant well distributed throughout waste and repository, like situation prior to intrusion 2. Addition of vast amounts of Castile brine does not substantially alter the solubility of either Pu ^{III} and Pu ^{IV} or U ^{IV} and U ^{VI}
Adsorption	Geochemical Constraint on Adsorption Concentration Similar to situation prior to intrusion
Colloid Filtration	Geochemical Constraint on Colloid Filtration Concentration 1. Although brine flow can stir up colloids, filtration of suspended colloids would be localized to microenvironments. These microenvironments would be well distributed on a macroscopic scale throughout repository and thus only recreate small agglomerations 2. Colloidal filtration/agglomeration of rust colloids, a likely colloidal substrate for fissile material, not critical since adsorption on homogeneous mixture of rust not critical 3. No bioaccumulation by microbes, like situation prior to intrusion.
Intrusion Culebra Fluid Flow	Hydrologic Constraint on Deposition Location in Culebra after Intrusion 1. Relatively greater permeability to other strata favors deposition in Culebra 2. Fluid tends to flow into Culebra rather than out of Culebra; thus, no deposition in adjacent strata 3. Low solubility of ²³⁹ Pu and ²³⁵ U fissile material requires vast amounts of brine; yet, mixing zone of Salado/Castile brine carrying fissile material into Culebra dolomite too large to reach 3.7 kg/m ³ Pu solid concentration or 180 kg/m ³ U solid concentration 4. Variability in brine flux up the borehole spreads out mixing zone in Culebra dolomite; specifically, solubility of Pu ^{III} decreases in Culebra dolomite when repository brines mix with Culebra brine but hydraulic constraint of moving mixing zone reduces tendency to precipitate Pu ^{III} in high concentrations.

Scenario <i>Location</i> Process	Rationale for Hydrologic/Geochemistry Not Causing Criticality
Intrusion <i>Culebra</i> Precipitation	Geochemical Constraint on Precipitation Concentration in Culebra after Intrusion <ol style="list-style-type: none"> 1. U ore deposits in evaporates, such as dolomite, are rare because carbonate in the formations increases rather than decreases solubility 2. At 5% enrichment, 180 kg/m³ critical concentration for UO₂ in Culebra far exceeds concentrations found in economically mineable ores (14 kg/m³ for 20%wt high-grade ore at 3000 ppm in dolomite) 3. Solubility of Pu^{IV} increases with the carbonate abundantly available in the Culebra dolomite brine; hence, reducing agent is necessary 4. No strong reductants (or oxidants) known in Culebra 5. At 100% enrichment, 3.7 kg/m³ critical concentration in Culebra dolomite and Culebra brine for Pu^{III} or Pu^{IV} requires concentrations exceeding low-grade ores (i.e., 2.4 kg/m³ for 1%wt low-grade ore at 1000 ppm) 6. Solubility of Pu^{III} decreases in Culebra dolomite when repository brines mix with Culebra brine but large and moving mixing zone reduces tendency to precipitate Pu^{III} in high concentrations.
Adsorption	Geochemical Constraint on Adsorption Concentration <ol style="list-style-type: none"> 1. Critical concentration of 3.7 kg/m³ requires entire adsorptive capacity of dolomite 2. Adsorption not exclusive to fissile Pu; other metal cations such as Ca⁺² and Mg⁺² in brine solution already occupy sites; hence, Pu must dislodge already adsorbed metal cations. 3. Adsorption and precipitation likely occur in different areas; adsorption tends to occur next to borehole, while precipitation occurs at away from borehole in mixing zone between Culebra and repository brines
Colloid Destabilization/ Filtration	Geochemical Constraints on Colloidal Destabilization/Filtration Concentration <ol style="list-style-type: none"> 1. Filterable mineral and microbial colloids adsorb Pu externally; thus, adsorption controlled by solution concentration 2. Equilibrium of the dissolved concentration with colloids within a small destabilization/filtration region limits the ability of colloids to exceed the solution concentration by many orders of magnitude. For simulations with Pu concentration at its maximum from extreme uncertainty, the filterable colloid fraction is miniscule. For simulation with Pu dissolved concentration at its mean, the filterable colloid fraction is only 28% of the total Pu concentration. 3. Colloidal destabilization occurs primarily because of changes in ionic strength which occur over large brine mixing zone too large to cause criticality (like precipitation) 4. To exceed critical concentration at mean values of Pu concentration, colloids must filter at borehole (like adsorption); yet the filterable fraction barely approaches the minimum critical mass and the critical concentration associated with the minimum critical mass cannot be reached.

ACKNOWLEDGMENTS

Sandia National Laboratories (SNL) is a multimission laboratory managed and operated by National Technology and Engineering Solutions of Sandia, LLC., a wholly owned subsidiary of Honeywell International Inc., for the DOE National Nuclear Security Administration under contract DE-NA0003525.

REFERENCES

1. R. P. RECHARD, L. C. SANCHEZ, H. R. TRELLE and C. T. STOCKMAN, "Unfavorable Conditions for Nuclear Criticality Following Disposal of Transuranic Waste at the Waste Isolation Pilot Plant," *Nuclear Technology*, **136**(1), 99-129 (2001).
2. R. P. RECHARD, L. C. SANCHEZ, C. T. STOCKMAN and H. R. TRELLE, "Consideration of Nuclear Criticality When Disposing of Transuranic Waste at the Waste Isolation Pilot Plant," SAND99-2898, Sandia National Laboratories (2000).

3. R. P. RECHARD, "Probability and Consequences of Nuclear Criticality at a Geologic Repository--I: Conceptual Overview for Screening," *Nuclear Technology*, **190**(2), 97-126 (2015).
4. DOE (US DEPARTMENT OF ENERGY), "Surplus Plutonium Disposition, Record of Decision," *Federal Register*, **81**(65), 19588-19594 (2016).
5. R. P. RECHARD, L. C. SANCHEZ, M. OLGVUN and G. RYBA, "Fissile Mass and Concentration Necessary for Criticality in Geologic Media near Bedded Salt Repository, Memorandum to Paul E. Shoemaker, 8880; Todd Zeitler, 8862; Ross Kirkes, 8883; November 2019," Sandia National Laboratory (2019).
6. R. P. RECHARD, L. C. SANCHEZ, P. K. MCDANIEL, J. HUNT and G. BROADOUS, "Fissile Mass and Concentration Criteria in Geologic Media near Bedded Salt Repository " *International High-Level Radioactive Waste Management Conference, April 14-18, 2019, Knoxville, TN, La Grange Park, IL: American Nuclear Society* (2019).
7. R. P. RECHARD, "Improbability of Transuranic Waste Compaction by Salt Creep Causing Criticality in Bedded Salt Repository; Memorandum to Paul E. Shoemaker, 8880; Todd Zeitler, 8863; Ross Kirkes, 8883; November 2019," Sandia National Laboratories (2019).
8. PUB. L. 97-425, "Nuclear Waste Policy Act of 1982," 96 Stat. 2201; 42 U.S.C. 10101 et seq. (1983).
9. EPA (US ENVIRONMENTAL PROTECTION AGENCY), "40 CFR Part 191: Environmental Standards for the Management and Disposal of Spent Nuclear Fuel, High-Level and Transuranic Radioactive Wastes: Final Rule," *Federal Register*, **50**(182), 38066-38089 (1985).
10. EPA (US ENVIRONMENTAL PROTECTION AGENCY), "40 CFR Part 191: Environmental Radiation Protection Standards for the Management and Disposal of Spent Nuclear Fuel, High-Level and Transuranic Radioactive Wastes, Final Rule," *Federal Register*, **58**(242), 66398-66416 (1993).
11. PUB. L. 102-579, "Waste Isolation Pilot Plant Land Withdrawal Act. (106 Stat. 4777)," (1992).
12. EPA (US ENVIRONMENTAL PROTECTION AGENCY), "40 CFR Part 194: Criteria for the Certification and Re-Certification of the Waste Isolation Pilot Plant's Compliance with the 40 CFR Part 191 Disposal Regulations; Final Rule," *Federal Register*, **61**(28), 5224-5245 (1996).
13. R. P. RECHARD, "Historical Background on Performance Assessment for the Waste Isolation Pilot Plant," *Reliability Engineering and System Safety*, **69**(1-3), 5-46 (2000).
14. EPA (US ENVIRONMENTAL PROTECTION AGENCY), "40 CFR Part 197: Public Health and Environmental Radiation Protection Standards for Yucca Mountain, Nevada; Final Rule," *Federal Register*, **66**(114), 32074-32135. US Environmental Protection Agency (2001).
15. EPA (US ENVIRONMENTAL PROTECTION AGENCY), "40 CFR Part 197: Public Health and Environmental Radiation Protection Standards for Yucca Mountain, Nevada; Final Rule," *Federal Register*, **73**(200), 61256:61289 (2008).
16. ANSI (AMERICAN NATIONAL STANDARDS INSTITUTE), "An American National Standard for Nuclear Criticality Safety in Operations with Fissionable Materials Outside Reactors," ANSI/ANS-8.1-2014, American National Standards Institute (2014).
17. M. G. MARIETTA, D. R. ANDERSON, G. BASABILVAZO, J. C. HELTON and H.-N. JOW, "Summary Discussion of the 1996 Performance Assessment for the Waste Isolation Pilot Plant," *Reliability Engineering and System Safety*, **69**(1-3), 437-452 (2000).
18. DOE (US DEPARTMENT OF ENERGY), "Title 40 CFR Part 191: Compliance Certification Application for the Waste Isolation Pilot Plant," DOE/CAO-1996-2184. Vol. I-XXI, DOE Carlsbad Area Office (1996).
19. EPA (US ENVIRONMENTAL PROTECTION AGENCY), "Criteria for the Certification and Re-Certification of the Waste Isolation Pilot Plant's Compliance with the 40 CFR Part 191 Disposal Regulations: Certification Decision," *Federal Register*, **63**(95), 27354-27406 (1998).
20. T. R. ZEITLER, B. A. DAY, J. BETHUNE, R. SARATHI and J. LONG, "Assessment of Abandoned Panel Closures in South End of Repository and Lack of Waste Emplacement in Panel 9," ERMS 568459, Sandia National Laboratories (2017).
21. R. P. RECHARD, M. L. WILSON and S. D. SEVOUGIAN, "Progression of Performance Assessment Modeling for the Yucca Mountain Disposal System for Spent Nuclear Fuel and High-Level Radioactive Waste," *Reliability Engineering and System Safety* **122**(2), 96-123 (2014).
22. EPA (US ENVIRONMENTAL PROTECTION AGENCY), "Compliance Application Guidance for 40 CFR 194," EPA-402-R-95-014, Office of Radiation and Indoor Air, US Environmental Protection Agency (1996).
23. R. P. RECHARD, "An Introduction to the Mechanics of Performance Assessment Using Examples of Calculations Done for the Waste Isolation Pilot Plant between 1990 and 1992," SAND93-1378 revised, Sandia National Laboratories (1996).

24. R. P. RECHARD, W. BEYELER, R. D. MCCURLEY, D. K. RUDEEN, J. E. BEAN and J. D. SCHREIBER, "Parameter Sensitivity Studies of Selected Components of the Waste Isolation Pilot Plant Repository/Shaft System," SAND89-2030, Sandia National Laboratories (1990).
25. M. G. MARIETTA, S. G. BERTRAM-HOWERY, D. R. ANDERSON, K. F. BRINSTER, R. V. GUZOWSKI, H. IUZZOLINO and R. P. RECHARD, "Performance Assessment Methodology Demonstration: Methodology Development for Evaluating Compliance with EPA 40 CFR 191, Subpart B, for the Waste Isolation Pilot Plant," SAND89-2027, Sandia National Laboratories (1989).
26. J. C. HELTON, F. J. DAVIS and J. D. JOHNSON, "Characterization of Stochastic Uncertainty in the 1996 Performance Assessment for the Waste Isolation Pilot Plant," *Reliability Engineering and System Safety* **69**(1-3), 167-189 (2000).
27. NRC (US NUCLEAR REGULATORY COMMISSION), "Yucca Mountain Review Plan, Final Report," NUREG-1804, REV 2, Office of Nuclear Material Safety and Safeguards, US Nuclear Regulatory Commission (2003).
28. C. D. LEIGH, J. TRONE and B. FOX, "TRU Waste Inventory for the 2004 Compliance Recertification Application Performance Assessment Baseline Calculation," ERMS 541118, Sandia National Laboratories (2005).
29. B. CRAWFORD, D. GUERIN, S. LOTT, W. MCINROY, J. MCTAGGART and G. D. VAN SOEST, "Performance Assessment Inventory Report--2008," INV-PA-08, Revision 0, Los Alamos National Laboratory, Carlsbad Operations (2009).
30. G. D. VAN SOEST, "Performance Assessment Inventory Report - 2012," INV-PA-12, Rev. 0; LA-UR-12-26643, Los Alamos National Laboratory Carlsbad Operations (2012).
31. G. D. VAN SOEST, "Performance Assessment Inventory Report--2018," INV-PA-18, Revision 0, Los Alamos National Laboratory (2018).
32. D. E. MUNSON, A. F. FOSSUM and P. E. SENSENY, "Advances in Resolution of Discrepancies between Predicted and Measured in Situ WIPP Room Closures," SAND88-2948, Sandia National Laboratories (1989).
33. C. T. STOCKMAN, J. W. GARNER, J. C. HELTON, J. D. JOHNSON, A. SHINTA and L. N. SMITH, "Radionuclide Transport in the Vicinity of the Repository and Associated Complementary Cumulative Distribution Functions in the 1996 Performance Assessment for the Waste Isolation Pilot Plant," *Reliability Engineering and Systems Safety*, **69**(1-3), 369-396 (2000).
34. L. BRUSH, H. "Test Plan for Laboratory and Modeling Studies of Repository and Radionuclide Chemistry for the Waste Isolation Pilot Plant," SAND90-0266, Sandia National Laboratories (1990).
35. H. W. PAPENGUTH and Y. K. BEHL, "Test Plan: Evaluation of Dissolved Actinide Retardation at the Waste Isolation Pilot Plant," TP 96-02. WPO 31336, Sandia National Laboratories (1996).
36. S. C. BABB and C. F. NOVAK, "FMT, Version 2.0, User's Manual," WPO 28119, Sandia National Laboratories (1995).
37. T. J. WOLERY, "EQ3/6, a Software Package for Geochemical Modeling of Aqueous Systems: Overview and Installation Guide (Ver. 7)," UCRL-MA-110662, Lawrence Livermore National Laboratory (1992).
38. Y. XIONG, "Release of EQ3/6 Database Data0.Fm1. E-Mail to Jennifer Long, March 9, 2011," ERMS 555152, Sandia National Laboratories (2011).
39. P. V. BRADY, H. W. PAPENGUTH and J. W. KELLY, "Metal Sorption to Dolomite Surfaces," *Appl. Geochem.*, **14**(5), 569 (1999).
40. D. LANGMUIR, *Aqueous Environmental Geochemistry*, Prentice Hall, (1997).
41. L. BRUSH, H and P. S. DOMSKI, "Prediction of Baseline Actinide Solubilities for the WIPP CRA-2014 PA," AP-153, Rev. 1 records package, Sandia National Laboratories (2014).
42. J. C. HELTON, J. BEAN, J.E., J. W. BERGLUND, F. J. DAVIS, K. ECONOMY, J. W. GARNER, J. D. JOHNSON, R. J. MACKINNON, J. MILLER, D. G. O'BRIEN, J. L. J. RAMSEY, J. D. SCHREIBER, A. SHINTA, L. N. SMITH, D. M. STOELZEL, C. T. STOCKMAN and P. VAUGHN, "Uncertainty and Sensitivity Analysis Results Obtained in the 1996 Performance Assessment for the Waste Isolation Pilot Plant," SAND98-0365, Sandia National Laboratories (1998).
43. Y. XIONG and P. S. DOMSKI, "Uncertainty Analysis of Actinide Solubilities for CRA 2014 Sensitivity Investigation Number 4," ERMS 567306, Sandia National Laboratories (2016).
44. H. W. PAPENGUTH and R. C. MOORE, "Attachement A: Rationale for Definition of Parameter Values for Mineral Fragment Type Colloids," WPO 35855, Sandia National Laboratories (1996).
45. H. W. PAPENGUTH, "Attachment A: Rationale for Definition of Parameter Values for Actinide Intrinsic Colloids," WPO 35852, Sandia National Laboratories (1996).

46. H. W. PAPENGUTH and R. C. MOORE, "Attachment A: Rationale for Definition of Parameter Values for Humic Substances," WPO 35855, Sandia National Laboratories (1996).
47. H. W. PAPENGUTH, "Attachment A: Rationale for Definition of Parameter Values for Microbes," WPO 35856, Sandia National Laboratories (1996).
48. DOE (US DEPARTMENT OF ENERGY), "Title 40 CFR Part 191 Subparts B and C Compliance Recertification Applicatin 2014 for the Waste Isolation Pilot Plant, Appendix SOTERM-2014 Actinide Chemistry Source Term," DOE/WIPP-14-3503, US Department of Energy, Carlsbad Field Office (2014).
49. C. HANSEL, M., S. G. BENNER and S. FENDORF, "Competing Fe(II)-Induced Mineralization Pathways of Ferrihydrite," *Environmental Science Technology*, **39**(18), 7147-7153 (2005).
50. Y. CUDENNEC and A. LECERF, "The Transformation of Ferrihydrite into Goethite or Hematite, Revisited," *Journal of Solid State Chemistry*, **179**, 716-722 (2006).
51. C. LIU, Z. ZHU, F. LI, T. LIU, C. LIAO, J.-J. LEE, K. SHIH, L. TAO and Y. WU, "Fe(II)-Induced Phase Transormation of Ferrihydrite: The Inhibition Effects and Stabilization of Divalent Metal Cations," *Ghemical Geology*, **444**, 110-119 (2016).
52. A. L. SANCHEZ, J. W. MURRAY and T. H. SIBLEY, "The Adsorption of Plutonium IV and V on Goethite," *Geochim. Cosmochim. Acta.*, **49**, 2297 (1985).
53. I. R. TRIAY, A. MEIJER, J. L. CONCA, K. S. KUNG, R. S. RUNDBERG, B. A. STRIETELMEIER, C. D. TAIT and R. C. ECKHARDT, "Summary and Synthesis Report on Radionuclide Retardation for Theyucca Mountain Site Characterization Project," Milestone Report 3784M. LA-13262-MS., Los Alamos National Laboratories (1997).
54. P. N. SWIFT and T. F. CORBET, "The Geologic and Hydrogeologic Setting of the Waste Isolation Pilot Plant.," *Reliability Engineering and System Safety*, **69**(1-3), 47-58 (2000).
55. T. CORBET, "Expedited CCA Activity: Geochemistry/Hydrology Issue in Culebra," WPO 42315, Sandia National Laboratories (1996).
56. K. G. BELL, "Uranium in Carbonate Rocks," Professional Paper 474-A, US Geological Survey (1963).
57. R. M. HOLT, "Conceptual Model for Transport Processes in the Culebra Dolomite Member, Rustler Formation," SAND97-0194, Sandia National Laboratories (1997).
58. J. A. DAVIS and D. B. KENT, "Surface Complexation Modeling in Aqueous Geochemistry." In *Mineral-Water Interface Geochemistry*, M.F. Hochella, Jr., and A.F. White (Eds.) Mineralogical Society of America (1990).
59. K. F. ECKERMAN, A. B. WOLBARST and C. B. RICHARDSON, "Limiting Values of Radionuclide Intake and Air Concentration and Dose Conversion Factors for Inhalation, Submersion, and Ingestion," EPA 520/1-88-020. Federal Guidance Report No. 11, US Environmental Protection Agency (1988).
60. C. M. STONE, "SANTOS - a Two-Dimensional Finite Element Program for the Quasistatic, Large Deformation, Inelastic Response of Solids," SAND90-0543, Sandia National Laboratories (1997).
61. P. VAUGHN, J. E. BEAN, J. C. HELTON, M. E. LORD, R. J. MACKINNON and J. D. SCHREIBER, "Representation of Two-Phase Flow in the Vicinity of the Repository in the 1996 Performance Assessment for the Waste Isolation Pilot Plant," *Reliability Engineering and System Safety*, **69**(1-3), 205-226 (2000).
62. G. E. HAMMOND, P. C. LICHTNER and R. T. MILLS, "Evaluating the Performance of Parallel Subsurface Simulators: An Illustrative Example with PFLOTRAN," *Water Resources Research*, **50** (2014).
63. M. FENG and T. LAFORCE, "Qualification Test for PFLOTRAN," ERMS 572028, Sandia National Laboratories (2019).
64. K. KUHLMAN, "Analysis Report for the CRA-2009 PABC Culebra Flow and Transport Calculations," AP-144, ERMS 552951, Sandia National Laboratories (2010).